Fuel Processing Technology 197 (2020) 106199

Contents lists available at ScienceDirect

Fuel Processing Technology

journal homepage: www.elsevier.com/locate/fuproc

From agriculture residue to upgraded product: The thermochemical conversion of sugarcane bagasse for fuel and chemical products

Caroline Carriel Schmitt[a,*], Renata Moreira[b], Renato Cruz Neves[c], Daniel Richter[a], Axel Funke[a], Klaus Raffelt[a], Jan-Dierk Grunwaldt[a,d], Nicolaus Dahmen[a]

[a] Institute of Catalysis Research and Technology (IKFT) – Karlsruhe Institute of Technology (KIT), Karlsruhe, Germany
[b] Fuels and Lubricants Laboratory (LCL) – Institute for Technological Research (IPT), São Paulo, Brazil
[c] Brazilian Bioethanol Science and Technology Laboratory (CTBE), Campinas, Brazil
[d] Institute for Chemical Technology and Polymer Chemistry (ITCP) – Karlsruhe Institute of Technology (KIT), Germany

ARTICLE INFO

Keywords:
Sugarcane bagasse
Biorefinery
Fast pyrolysis bio-oil
Catalytic upgrading
Nickel-based catalyst

ABSTRACT

A holistic investigation considering the sugarcane bagasse characterization, fast pyrolysis and upgrading of bio-oil applying two nickel-based catalysts is presented. The bio-oil composition is correlated to the bagasse building blocks, and the hydrotreatment reaction pathways are identified. Despite the high ash content of 6.75 wt%, 60.1 wt% of bio-oil was obtained by fast pyrolysis, attributed to low concentration of potassium (0.08 wt%) and low humidity (2.80 wt%) observed in the bagasse. Upgraded bio-oil with 60.3% less water and 43.3% less oxygen were obtained with Ni/SiO_2, resulting in an HHV 63% higher compared to bagasse. $Ni\text{-}Cr/SiO_2$ showed the highest hydrogenation activity and the highest conversion of acids, converting 25.7% of acetic acid and 14.95% of propionic acid while Ni/SiO_2 was more active for conversion of compounds containing aromatic groups. The higher viscosity of upgraded oils in comparison to the fast pyrolysis bio-oil indicates that the stabilization during the heating ramp can be improved to suppress polymerization. Hence, sugarcane bagasse is an attractive feedstock with an overall final yield of 30.5 wt% of the upgraded product.

1. Introduction

Sugarcane crops play a significant role in sugar and ethanol production worldwide. The annual production around the globe was recently estimated in approximately 1.6 billion tons [1], mainly used for sugar and ethanol production by fermentation (first generation ethanol (1G)). Brazil, considered the biggest sugarcane producer in the world, has an approximate production in 2018/2019 of 635.51 million tons of sugarcane with 30.41 billion of litre of ethanol produced [2]. Considering that for each ton of sugarcane produced, 0.28 tons of sugarcane bagasse (SCB) are generated [3], 448 million tons of bagasse are generated annually worldwide. Approximately 178 million tons are generated in Brazil. Usually the bagasse is destined for bioelectricity generation, mostly used in the production unit, with the surplus transferred to the electric grid [4,5]. New alternatives have been studied in the last years, in order to use the sugarcane bagasse as a feedstock for ethanol production, so called second generation (2G) ethanol by making use of the feedstock's polycarbohydrates. 1G ethanol production is relatively simple compared to the complex 2G ethanol, which requires first separation from the lignin fraction, hydrolysis and then the fermentation of monomers to ethanol [6,7]. Many efforts are being dedicated in order to reduce the costs and increase the efficiency of the second generation ethanol [5,6].

An alternative for sugarcane bagasse conversion is the 2G thermochemical conversion, e.g. by fast pyrolysis. To carry out fast pyrolysis, the dry biomass (moisture content below 10 wt%) is ground to a particle size of < 3 mm, thermally decomposed at approximately 500 °C in inert atmosphere with a hot gas residence time of a few seconds, resulting in a fast pyrolysis bio-oil (FPBO) as the main product [8,9]. FPBO is a brown liquid with high water content and high viscosity [10]. In contrast to fermentation products, the pyrolysis oil is composed of hundreds of oxygenated compounds such as carboxylic acids, ketones, aldehydes, alcohols, phenols, sugars, ethers, and esters already identified [10–13]. FPBO can be used to supply power and heat or it can be further processed towards fuel and chemical products [9,14].

Relatively clean (i.e. ash-free) wood is the state-of-the-art feedstock for industrial applications of fast pyrolysis. A variety of other types of biomass have been applied as feedstocks for FPBO production, such as wheat straw [15], corn stover [16], palm empty fruit bunches [17] and many other biomasses such as pine wood or switchgrass and rice straw

* Corresponding author.
E-mail address: caroline.schmitt@partner.kit.edu (C.C. Schmitt).

https://doi.org/10.1016/j.fuproc.2019.106199
Received 4 June 2019; Received in revised form 7 August 2019; Accepted 26 August 2019

[18]. Some studies performed with sugarcane bagasse do exist for the case of slow pyrolysis [17,19,20], but there is little information on fast pyrolysis of SCB [8].

Although the use of different types of biomass results in FPBO with different compositions [9,17,21], in general, the FPBO show similarities. FPBO has approximately half of the heating value of crude oil, shows high acidity (pH value below 3), high water concentration (15–35 wt%), polymerization due to secondary reactions which results in aging phenomena, and high oxygen content (35–50 wt%), which limits its direct application as boiler fuel [9,11,22]. Consequently, if application as a transportation fuel or even some chemicals in the context of a bio-based refinery is targeted, upgrading is required.

Different strategies are used for FPBO upgrading and conditioning: solvent addition for viscosity reduction, emulsification or extraction with diesel fuel, esterification, hydrotreatment and others [9]. The hydrotreatment is performed at high pressures of hydrogen, and applying catalysts aiming at stabilization and hydrodeoxygenation of the FPBO [11,23]. In this way, the FPBO can be practically completely deoxygenated to hydrocarbons and/or partially deoxygenated to a range of fuel intermediates or profitable chemicals [11,12,24]. Hence, the catalyst plays an important role in the hydrotreatment reactions. For that reason, the choice and development of catalyst for FPBO hydrotreatment has been a subject of many investigations. Particularly nickel-based catalysts showed to be active for conversion of model compounds [25–28] and fast pyrolysis bio-oil of different feedstocks [29,30]. Additionally to the low cost, high degree of deoxygenation, possibility of inclusion of promoters in the catalyst formulation whether for different selectivity [31] or higher resistance to poisoning substances and deactivation [32] have been previously reported as advantages of nickel-based catalysts.

Although some groups have already considered the pyrolysis of sugarcane bagasse, only very few have worked on the hydrotreatment of the liquid product fraction [33] and up to now not considered the whole process chain from SCB. However, this represents an essential step in order to evaluate the viability of the 2G thermochemical conversion integration to the 1G ethanol unit depicted in Fig. 1. The use of SCB is especially advantageous in comparison to other biomasses or sugarcane leaves, as it is already centrally collected in the sugar mill. Sugarcane leaves are usually left in the field, requiring an efficient and cheap collection system [6,34]. Hence, the centralized sugarcane conversion unit would be beneficial from an economic point of view, allowing bigger scale units, without the need to transport the feedstock or an intermediate product, as usually suggested for biomass derived bio-oils production [21]. Additionally, the high concentration of lignin (17–32 wt%) [34,35], considered a limitation for carbohydrate hydrolysis [34] makes the sugarcane bagasse especially interesting for thermochemical valorisation [36], as not just hydrocarbons but also functionalized aromatics monomers are interesting target products [24]. This approach is especially relevant for countries such as Brazil, with record production of sugarcane ethanol in 2019 and perspective of increased production until 2030 [37]. The high volumes of agriculture residues generated, can undergo thermochemical conversion followed by hydrotreatment, resulting in products with potential to be blended to aviation kerosene, in the concentration of 10%, as defined by the Brazilian national biofuel policy (RenovaBio) for 2030 [38]. Furthermore, a new range of functionalized chemicals, i.e. functionalized aromatic compounds can be produced, expanding the range of chemicals obtained in the sugarcane refinery.

The aim of this study is to present for the first time a comprehensive investigation, from the bagasse characterization, followed by fast pyrolysis and hydrotreatment to the final upgraded products. The experimental work is conducted in the same laboratory and analytical methods are aligned so that maximum consistency is achieved. Specific focus is set on conversion of SCB by fast pyrolysis to maximize organic liquid yield, subsequent hydrotreatment of the produced FPBO, correlation between the sugarcane bagasse building blocks and the main compounds observed in the bio-oil. Additionally, the main chemical reactions taking place during the hydrotreatment are identified and discussed. This approach allows identification of feedstock specific characteristics, advantages, and disadvantages of the whole process chain.

2. Material and methods

2.1. Sugarcane bagasse collection, preparation and characterization

The sugarcane bagasse was collected at Iracema biorefinery, located in Iracemápolis, São Paulo, Brazil, in June 2016. The SCB was pre-dried

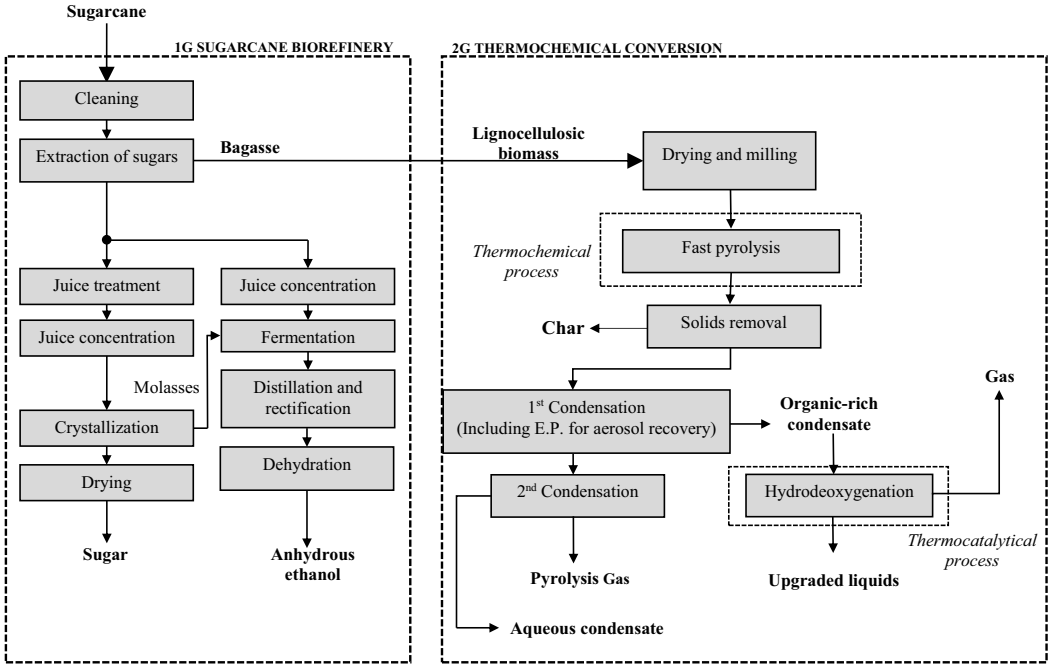

Fig. 1. Integration of 1G and 2G thermochemical conversion route for sugarcane biorefinery. E.P: Electrostatic precipitator.

at 105 °C overnight (FABBE oven) to a moisture content of 46.2%. This procedure was performed at IPT (Institute for Technological Research, São Paulo, Brazil). In the sequence, the samples were shipped to Germany in plastic bags.

The SCB was further dried in Germany for 3 days at room temperature (moisture content below 10 wt%), chopped (Viking GE260) and milled to ≤2 mm with a cross-beater mill SK100. Approximately one third of the sample was further milled to fine powder using a cryogenic mill (Freezer/Mill® Cryogenic grinder 6875), in order to be characterized in terms of moisture and ash content, elemental analysis, volatile matter, higher heating value and major elements. Pictures of dry and milled SCB are depicted in the Supplementary Material (Fig. S.1a and S.1b).

The moisture and ash content were determined using a thermogravimetric analyzer (TGA 701, LECO). For moisture determination, the sample was maintained at constant temperature of 105 °C in air until constant weight (mass loss is then attributed to the sample's moisture content). The ash content was obtained under the following conditions: the sample was heated from ambient to 250 °C at a heating rate of 4.5 °C/min and maintained at this temperature for 30 min. In the sequence, the SCB was heated to 550 °C ± 10 °C at a heating rate of 10 °C/min and maintained at this temperature for 120 min. The residue is then considered as the ash content.

The volatile matter content was obtained placing 1 g of sample for seven min in a furnace (Nabertherm model LV9/11) at 900 °C ± 10 °C. The volatile matter is the difference between the sample's weight before and after the thermo treatment.

The higher heating value (HHV) was determined using the calorimeter IKA C 5000 at 25 °C and at constant volume. Carbon, hydrogen and nitrogen content were determined using a CHN 628 Leco. Sulfur content was obtained by Eltra CS-2000 elemental analyzer. The concentration of oxygen was calculated by difference, as follow:

$$[O]_{wt\%} = 100 - ([C]_{wt\%} + [H]_{wt\%} + [N]_{wt\%} + [S]_{wt\%} + [ash]_{wt\%}) \quad (1)$$

The fixed carbon content (FC) was obtained by the difference considering the moisture, ash and volatile matter content.

$$FC_{wt\%} = 100 - M_{wt\%} - A_{wt\%} - VM_{wt\%} \quad (2)$$

where M is the moisture content, A is the ash content and VM is the volatile matter content in weight percent.

Major inorganic elements (Al, Ca, Fe, Mg, P, K, Si, Na and Ti) present in the SCB were quantified by ICP-OES (Agilent 725, Inductively Coupled Plasma Emission Spectrometer). The samples were prepared by microwave digestion (Anton Paar, Multiwave 3000) by mixing approximately 0.5 g of dry bagasse with 6 ml of HNO_3 (65 vol%, Merck Millipore), 2 ml HCl (37 vol%, Merck Millipore), 1 ml HF (40 vol%, Merck Millipore) and 0.5 ml of H_2O_2 (35 vol%, Merck Millipore). The digestion is performed at 240 °C for 1 h.

Additionally, the SCB was characterized by Py-GC/FID (pyrolysis gas chromatography/flame ionization detector) and by Py-GC/MS (pyrolysis gas chromatography/mass spectrometer) at Instituto Superior de Agronomia (ISA), University of Lisbon, Portugal. For the Py-GC/FID measurements, approximately 76 mg of sample was pyrolyzed by a CDS Pyroprobe 1000 (650 °C, 10 s), coupled to a gas chromatograph (Agilent 7820) by a heated interface at 270 °C. The compounds were injected at 270 °C (split 1:20), separated in a low/mid-polarity column (J&W Scientific DB-1701, 60 m × 0.25 mm × 0.25 μm), and detected by a FID detector at 270 °C. The oven was programmed starting at 45 °C for 4 min, heated to 270 °C at a heating rate of 4 °C/min and kept at this temperature for 6 min. The area of each peak was used for quantification of compounds [39]. The qualification of the pyrolysis products was performed by a HP 6890 connected to an Agilent 5973 MS detector (sample pyrolysed by a CDS Pyroprobe 100 as described previously). The compounds were identified by comparison with literature and the NIST library. More information regarding the methodology can be found elsewhere [40].

2.2. Fast pyrolysis

The SCB conversion was performed at the Python process development unit located at the Institute of Catalysis Research and Technology, Karlsruhe, Germany. More details regarding the fast pyrolysis unit (feedstock conversion capacity of 10 kg/h of biomass) as well as the method description can be found elsewhere [41]. The dry biomass was used as obtained from < 2 mm screening after milling in a cross beater mill. In the pyrolysis unit, the feedstock was mixed with preheated heat carrier (1 mm steel beads) in a twin-screw mixer reactor. The mechanical mixing is designed to ensure the high heating rate required for fast pyrolysis at around 500 °C [42,43]. After pyrolysis, solids are recovered from gas cyclones at reactor temperature before the gas phase is recovered from two condensers. The first condenser is designed as a quench system to instantly cool down the gas phase from reactor temperature to around 90 °C. In this stage an organic-rich condensate is collected, further cooled down and recirculated to act as quenching medium for the incoming hot pyrolysis vapor. The second condenser is operated at ambient temperature at around 20 °C to obtain the water rich aqueous condensate. The condensate is also recirculated to the condenser after cooling to form a film inside its tube bundle, i.e. there is direct contact of incoming pyrolysis gas and recirculated condensate. The remaining non-condensable gas is vented after analysis by a GC/FID (Emerson, Daniel Modell 700).

The FPBO samples collected for subsequent hydrotreatment have been obtained from a modified condensation system which was

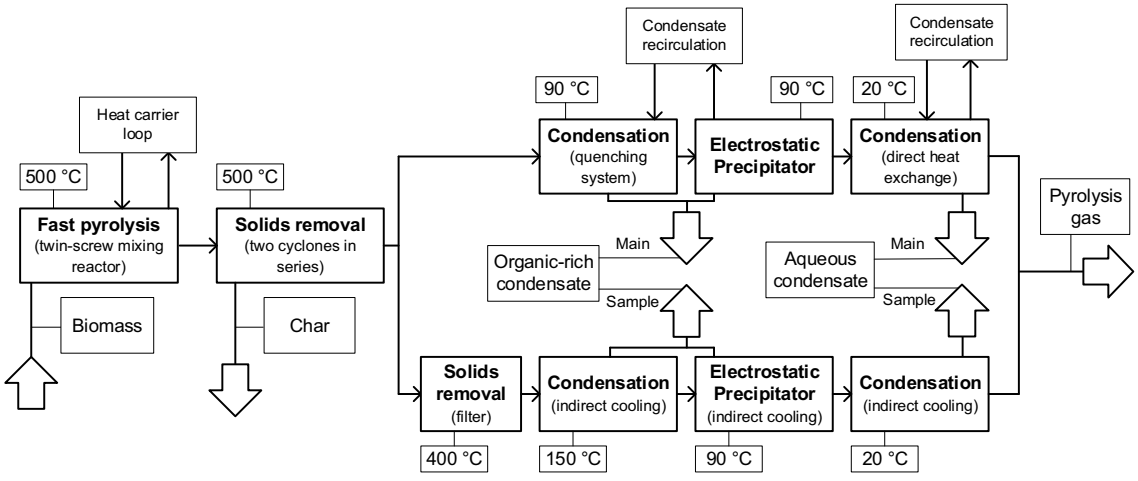

Fig. 2. Block flow scheme of the pyrolysis and the product (upper line) and sample (lower line) recovery system.

operated parallel to the main pyrolysis product flows (see Fig. 2). The reason for this procedure is the fact that both condensation loops require a start-up material to initiate condensation (ethylene glycol and water for first and second condenser, respectively). This start-up material is not being displaced during one experimental day and thus represents a significant fraction of the obtained FPBO. The results of hydrotreatment would inevitably be obscured by the start-up material. Instead, hot pyrolysis gas is extracted between the cyclones and the first condensers at reactor temperature and condensed by indirect cooling. In this sampling train, hot gases initially pass a ceramic filter (operated at 400 °C) to remove remaining particles. Most of the sensible heat is removed in a jacketed tube operated with cooling water. The gases leave this condenser at around 100–150 °C despite the low cooling temperature. This first condensation step is followed by an electrostatic precipitator where aerosols are removed and the gas further cools down to the desired temperature (around 90 °C in analogy to the first condensation stage in the main system). Condensate of the first two condensation steps is merged in one collection vessel and represents the organic condensate. The aqueous condensate is obtained subsequently in a condenser with a cooling coil (operated at 4 °C) so that the outlet gas leaves slightly below 20 °C. Remaining gases are merged after the final condensation step and vented after analysis.

For subsequent hydrotreatment, only the organic condensate (Fig. S.1 c), obtained at 90 °C from the sampling train is used and further denoted as sugarcane bagasse fast pyrolysis bio-oil (SCBPO).

2.3. Hydrotreatment reactions, conditions and analysis

In order to upgrade the SCBPO, batch reactor experiments using different catalysts were performed. The hydrotreatment was performed using a self-designed and built 200 ml autoclave. The catalysts as well as the upgrading condition (325 °C and 90 bar of H_2) were selected as reference case used in our previous investigations [29,44]. Two Ni-based catalysts, one commercially available and the other prepared by wet impregnation technique at IKFT, were used for the upgrading reactions. The commercially available catalyst is composed of 30 wt% of Ni, 26 wt% of NiO, 1.5 wt% graphite and 15 wt% of Cr_2O_3, supported on diatomaceous earth (mainly composed by SiO_2) with a specific surface area of 94 m^2/g. The commercially available catalyst is denoted as Ni-Cr/SiO_2 in the following. The second catalyst, denoted Ni/SiO_2 (7.9 wt% Ni, specific surface area of 215 m^2/g), was prepared by wet impregnation in a rotary evaporator (Hei-VAP Advantage ML/G3). More details are given in the Supplementary Material (S.k).

Approximately 50 g of SCBPO was mixed with 2.5 g of catalyst in the autoclave. The mixture was purged with nitrogen for 5 min and then pressurized with H_2 (Air Liquide ALPHAGAZ 2, 6.0) at ambient temperature to 90 bar. The reactor was heated at 5 °C/min until 325 °C and constantly mixed along the reaction (gas injector stirrer at 1000 rpm). The overall reaction time was around 120 min, including the heating ramp. Due to the limited amount of SCBPO, a single hydrotreatment reaction was performed for each condition tested. Once the reaction was finished, the reactor was cooled down with a flow of compressed air to approximately 50 °C and further cooled down to ambient temperature (approximately 25 °C) using an ice/water bath. A gas sample was collected for quantification of the main gaseous products and hydrogen by gas chromatography (GC-TCD/FID Agilent 789A, columns Restek 57,096 and Resteck Molsieve 5A). More information is given in the Supplementary Material (c). In addition, the H_2 consumption was calculated using the ideal gas equation, the hydrogen concentration given by GC-TCD/FID as well as the reactor's pressure registered before and after reaction [45]. The remaining liquid and solid fractions were collected, centrifuged (7000 rpm, 40 min, Thermo Fisher Heraeus Biofuge Stratos) and separated. The reactions conducted with Ni/SiO_2 resulted in two upgraded liquid phases, a upgraded light phase (ULP) and heavier oil, denominated upgraded oil phase (UOP). The reactions conducted with Ni-Cr/SiO_2 resulted in three liquid phases: ULP, an intermediate upgraded phase (IUP), and UOP. The liquid samples (ULP, IUP, UOP as well as SCPBO) were characterized in terms of elemental analysis (CHN 628 Leco), pH (Metrohm pH-meter 691), water content (Metrohm, Karl Fischer Tritando 841), higher heating value (IKA C 5000 1/10 Control Calorimeter) and sulfur (Agilent Inductively Coupled Plasma Emission Spectrometer 725). The higher heating values presented in dry basis were calculated based on Channiwala's equation [46]:

$$\mathrm{HHV(MJ/kg)} = 0.3491 \times \mathrm{C} + 1.1783 \times \mathrm{H} - 0.1034 \times \mathrm{O} - 0.0151 \times \mathrm{N} + 0.1005 \times \mathrm{S} - 0.0211 \times \mathrm{ash} \quad (3)$$

In order to further understand the chemical composition of the upgraded liquids in comparison to the SCBPO, a qualitative investigation was performed by GC/MS HP G1800A. The samples were prepared by dilution in methanol (1:20 or 1:10), filtrated (0.25 µm polytetrafluoroetylene filter) and 1 µl was injected at 250 °C (injector temperature) with split of 1:20. The oven was programmed to start at 40 °C maintained for 5 min, heated at a rate of 8 °C/min to 250 °C and maintained at this temperature for 10 min. The separation of the compounds was performed by a Restek stabilwax column (30 m × 0.25 mm × 0.25 µm).

A quantitative analysis of the main compounds in the SCBPO as well as in the upgraded products was performed by GC–MS/FID. The measurement was conducted at Thünen Institute in Hamburg, Germany. A volume of 1 µl of sample containing fluoranthene as internal standard was measured in a HP 6890. The sample is injected splitless at 250 °C (injector temperature), in a 14% cyanopropyl-phenyl-methylpolysiloxane column (60 m × 0.25 mm × 0.25 µm). The oven temperature started at 45 °C maintained for 4 min, heated to 280 °C at 4 °C/min and maintained at this temperature for 20 min. The GC was equipped with two parallel detectors: a FID and a MS detector (HP 5972). The qualitative analysis was performed comparing the compounds spectra with a NIST and a home-made library. Further information about the methodology can be found elsewhere [47].

Additionally measurements of viscosity, molecular weights, number average (Mn) and weight average (Mw) and polydispersity (Mw/Mn), obtained by Size Exclusion Chromatography (SEC) were performed. The dynamic viscosity measurements were conducted at Institute for Mechanical Process Engineering and Mechanics at KIT, using an Anton Paar rheometer at 40 °C. The SEC was performed at DWI Leibniz Institute for Interactive Materials in Aachen, Germany. The measurement was conducted using an HPLC pump (1260 Infinity II, Agilent), an UV-detector (UV-2075plus, Jasco), a refractive index detector (1290 Infinity II, Agilent) and a multi angle light scattering (MALS) (SLD 7100, Polymer Standards Service). Further information is available in the Supplementary Material (S.j).

The solid samples (composed by spent catalyst and solid residue), were separated from the liquid fractions by centrifugation. The residual solid in the autoclave was washed with acetone, collected and mixed with the solid from centrifugation. The samples (solid from autoclave + centrifugation), were then vacuum filtrated and washed several times with acetone, until all remaining UOP was completely removed. The spent catalyst was analyzed in terms of elemental composition, using the same methodology described for the liquid samples. Sulfur, nickel and chromium concentration were determined by ICP-OES sample preparation using a mixture of 2 ml of HNO_3 (37%, Merck Millipore), 6 ml of HCl (37%, Merck Millipore) and 0.5 ml of H_2O_2 (35%, Merck Millipore), followed by digestion in a Anton Paar, Multiwave 3000 microwave oven for 45 min at 240 °C) and crystalline structure analysis by powder X-ray diffraction (spectrometer X'Pert PRO MPD PANalytical instrument, cooper anode Cu Kα 1.54060 Å). The measurements were recorded in a 2 theta range of 5° to 120° for 1 h (step size 0.017°). The Scherrer equation was used for determination of the crystallite size (shape factor K = 0.9) after line broadening. Additionally, the fresh Ni-Cr/SiO_2 catalyst was analyzed by temperature programmed reduction using an Autochem HP 2950

(Micrometrics). The sample was previously dried in-situ in Ar flow of 30 mL/min for 3 h at a constant temperature between 200 °C. For the measurements, a flow of 30 ml/min of 5% H_2 in Ar was applied and a heating rate of 1 K/min until 400 °C. A mass spectrometer (MKS Cirrus 2) was used for recording TPR profiles. The H_2-TPR of Ni/SiO_2 can be found elsewhere [29]. The solid deposition over the catalyst was determined considering that it is mainly composed by carbon, as other compounds are considered negligible [29,48]. The carbon content in the spent catalyst, determined by elemental analysis (micro-elemental analyzer Elementar Vario el Cube) was used for the calculation as follow:

$$m_{solid} = ([C_{spcat}]_{wt\%} \times m_{cat})/(100 - [C_{spcat}]_{wt\%}) \quad (4)$$

where the m_{solid} is the mass of coke (g) in the spent catalyst; $[C_{spcat}]$ is the carbon deposited on the spent catalyst (wt%) obtained by elemental analysis and m_{cat} is the amount of catalyst (g) loaded to the reactor.

3. Results and discussion

3.1. Sugarcane bagasse characterization

The analytical results including the proximate and elemental analysis, inorganic compounds and other physicochemical properties are presented in Table 1.

The sugarcane bagasse showed low moisture content (2.80 wt%) when received for the analytics, after the drying process (see Section 2.1). The water content is one of the main parameters for biomass characterization, considering that the pyrolysis process can be affected and the efficiency reduced if the moisture content is > 10 wt% [20]. Hence, in this case the drying process was very successful. The high volatile matter observed (80.32 wt%) is an indication of the ability of the biomass to be devolatilized [49]. The SCB shows an ash content of 6.75 wt%. Compared to woody biomass, grassy biomass generally shows higher ash content, being responsible for lower liquid yields, high water and gas formation in the pyrolysis process [50–52]. Furthermore, high ash content and high fixed carbon results in high char formation [19]. The elemental analysis (Table 1) uncovers carbon, hydrogen and oxygen as main constituents, whereas sulfur and nitrogen are found to be lower in comparison to other studies. For example, Rabiu et al. [53] found sulfur and nitrogen concentrations of 0.80 wt% and 1.60 wt%, while Sukumar et al. [54] observed sulfur and nitrogen concentrations of 0.19 wt% and 0.69 wt%, respectively. As presented by Islam et al. [19] the concentration of these compounds can differ significantly among sugarcane samples. Sulfur is well known as a poisoning agent for catalysts [55] during the upgrading treatment step [29,56]. Hence, the lower concentration observed in this case can be considered an advantage, as the pyrolysis oil is expected to have lower sulfur in comparison to another residual biomasses, i.e. wheat straw [56,57]. Regarding the inorganic compounds identified, Si is present in highest amount, followed by iron and aluminum. Potassium is observed in smaller concentration (0.08 wt%), but still requires attention due to its catalytic activity during the pyrolysis process, reducing the liquid yield [9] and increasing char formation [36].

Table 1
Characterization results for the sugarcane bagasse.

	SCB[a]
Residual moisture (wt%)	2.80
HHV (MJ/kg)	18.51
Proximate analysis	
Ash (wt%)	6.75
Volatile matter (wt%)	80.32
Fixed carbon (wt%)	10.14
Elemental analysis	
Carbon (wt%)	47.40
Hydrogen (wt%)	6.14
Nitrogen (wt%)	0.28
Sulfur (wt%)	< 0.1
Oxygen (wt%)	46.18
Inorganic compounds	
Al (wt%)	0.11
Ca (wt%)	0.05
Fe (wt%)	0.19
K (wt%)	0.08
Mg (wt%)	0.04
Mn (wt%)	< 0.01
Si (wt%)	1.79
Ti (wt%)	0.04
Zn (wt%)	< 0.01

[a] Values are the average of two measurements. Methodologies performed accordingly to the standards described in Supplementary Material (Table S.1).

The characterization of SCB by Py-GC/MS and Py-GC/FID provides information about the main building blocks contributing to the lignocellulosic biomass composition [58]. A total of 71 compounds were detected (Table 2). Among them, 19 compounds were linked to polysaccharides (c), 7 compounds linked to hexoses (ch), 4 compounds to pentose (cp), 3 compounds to hydroxyphenyl (h), 22 compounds to guaiacyl (g), 9 compounds linked to syringyl (s) units while 7 peaks could not be precisely assigned. The pyrogram is available in the Supplementary Material (Fig. S.2 and Table S.2). Compounds derived from hexoses and polysaccharides were obtained with the highest relative abundance (Table S.2). Hydroxyacetaldehyde, the major compound identified (12.52%), is derived from cellulose depolymerization (ring fragmentation), in the same way as levoglucosan, obtained by transglycosylation of cellulose and one of the compounds with the highest relative abundance (6.12%) [59,60]. Compounds such as propanal-2-one (8.93%), acetic acid (8.19%) and 2-hydroxy-3-oxobutanal (4.46%) and hydroxypropanone (2.23%) derived from polysaccharides units [61], also showed high relative abundance.

The ring scission of holocellulose (cellulose and hemicellulose) results in ketones and aldehydes, such as propanal and 2-hydroxy-3-oxobutanal [62,63], observed in significant quantities. Acetic acid is mainly derived from hemicellulose (elimination of acetyl group linked to xylose) [60,64], but can be also formed by the cracking of lignin side chain as well as be formed as a by-product of levoglucosan scission [60,61]. Other compounds obtained from cellulose decomposition, as furans [62] were also observed among the products.

The high number of small volatile compounds observed can be a result of the pyrolysis temperature, leading to fragmentation to volatile products, mainly ketones and aldehydes [62], as observed (Table 2).

In addition, typical lignin derived compounds were identified [34,40,58,62,65,66] (Table 2 and Fig. 5). Guaiacyl derived compounds, such as guaiacol, 3-methylguaiacol, 4-methylguaiacol, eugenol and 4-vinylguaiacol corresponded to the majority of all lignin derived compounds, with major contribution of 4-vinylguaiacol (3.92%). Usually softwood lignin is rich is guayacyl units, as reported elsewhere [67]. The main syringyl derived compounds identified were syringol, 4-methylsyringol and 4-vinylsyringol while the hydroxyphenyl derived compounds were phenol, p-cresol and m-cresol.

The lignin content was calculated as the sum of the h + s + g peak areas divided by the sum of all peaks area. This method has been previously described elsewhere [40] and validated for woody biomass. Due to the differences in the feedstocks, the amount of lignin in the SCB sample was roughly estimated as 18 wt%, within the expected range [35] for this type of biomass. The syringyl/guaiacyl ratio of 0.49 is well in agreement with previous studies [68].

3.2. Fast pyrolysis

The fast pyrolysis reactions resulted mainly in liquid products (60.1 wt%), followed by non-condensable gas (19 wt%) and solids (13.5 wt%) (Table 3). The organic liquid yield, i.e. the liquid yield

Table 2
Compounds obtained by Py-GC of the SCB.

Compound	%[a]	Compound	%[a]
Acetaldehyde[c]	1.86	Eugenol[g]	0.26
2-Propenal (acrolein)[c]	1.95	4-Propylguaiacol[g]	0.07
Propanal[c]	8.93	5-Hydroxymethyl-2-furaldehyde[ch]	0.98
2,3-Butandione[c]	2.26	gamma-Lactone derivative[c]	0.53
Butanone-(2) or unknown[c]	1.37	Syringol[s]	1.21
Hydroxyacetaldehyde[ch]	12.52	Isoeugenol (cis)[g]	0.14
Acetic acid[c]	8.19	Pyran-(4H)-4-one, 2-hydroxymethyl-5-hydroxy-2,3-dihydro[ch]	1.35
Hydroxypropanone[ch]	2.23	1,5-Anhydro-b-D-xylofuranose[cp]	0.10
Unknown[u,c]	0.27	Isoeugenol (trans)[g]	0.54
3-Hydroxypropanal[c]	3.15	Syringol, 4-methyl-[s]	0.69
3-Butenal-2-one[c]	1.03	Vanillin[g]	0.75
(3H)-Furan-2-one[c]	0.98	Indene, 6-hydroxy-7-methoxy-, 1H-[g]	1.19
2-Hydroxy-3-oxobutanal[c]	4.46	Indene, 6-hydroxy-7-methoxy-, 2H- [g]	0.58
Furfural[c]	2.86	Homovanillin [g]	0.31
Dihydro-methyl-furanone[c]	3.95	Acetoguaiacone [g]	0.25
Isomer of 4-Hydroxy-5,6-dihydropyran-(2H)-one[cp]	1.43	Syringol, 4-vinyl-[s]	0.89
2(5H)-Furanone[c]	1.52	Guaiacyl acetone [g]	0.16
Gamma-Lactone and unknown[c]	0.24	Unknown[g/s]	0.25
4-Hydroxy-5,6-dihydropyran-(2H)-2-one[cp]	5.18	Propioguaiacone[g]	0.07
2-Hydroxy-1-methyl-cyclopenten-(1)-3-one[ch]	1.23	Isomer of coniferyl alcohol[g]	0.19
Phenol[h]	0.57	G−CO−CH=CH_2[g]	0.20
Guaiacol[g]	0.95	G−CO−CO−CH_3[g]	0.05
Methyl-butyraldehyde derivative[c]	0.61	1,6-Anydro-b-D-glucopyranose (levoglucosan)[ch]	6.12
p-Cresol[h]/	0.32	Syringol, 4-propenyl-(trans)[s]	1.37
m-Cresol[h]	0.07	Dihydroconiferyl alcohol[g]	0.11
3-Methylguaiacol[g]	0.24	Syringaaldehyde[s]	0.57
Gamma-lactone derivative[c]	1.49	Coniferyl alcohol (cis)[g]	0.16
4-Methyl guaiacol[g]	0.73	Homosyringaaldehyde[s]	0.17
Anhydrosugar[c]	1.44	Anhydrosugar: unknown[c]	0.42
Overlapping spectra; 4-ethyl-guaiacol[gc]	1.25	Acetosyringone[s]	0.32
Unknown[u,c]	0.45	Coniferyl alcohol (trans)[g]	0.07
Unknown[u,c]	0.31	Coniferylaldehyde[g]	0.76
1,4:3,6-Dianhydro-glucopyranose[ch]	0.28	Isomer of sinapyl alcohol	0.12
1,5-Anhydro-arabinofuranose[cp]	0.41	Sinapyl alcohol (trans)[s]	0.01
4-Vinylguaiacol[g]	3.92	Sinapinaldehyde[s]	0.40

[a] Calculated as follow: $[A_i/A_t] \cdot 100$ where A_i is the area of the peak of the compound i and A_t is the sum of the areas of all the compounds. The superscripts [c], [ch], [cp], [h], [g], [s] and [u] correspond to compounds derived from polysaccharides, hexoses, pentose, hydroxyphenyl, guaiacyl, syringyl and unknown, respectively.

excluding water, was 48.7 wt% on a dry feedstock basis. The results indicate that SCB is a very good feedstock for FPBO production – it yields almost as much organic liquids as poplar wood in the same experimental setup [42]. This high yield is observed despite the higher ash content of SCB as compared to the previously used poplar wood.

Table 3
Fast pyrolysis product yields and SCBPO physicochemical properties.

	Sugarcane bagasse fast-pyrolysis products
Mass Balance (as received basis)	
Solids (wt%)	13.5
Organic condensate (SCBPO) (wt%)	54.6
Aqueous condensate (wt%)	5.5
Gas (wt%)	19.0
Loss (wt%)	7.4
Physicochemical properties and elemental analysis - SCBPO (wet basis; dry basis)[a]	
Solid (wt%)	0.8
pH value	2.9
H_2O (wt%)	20.9
Density (g/cm^3)	1.18
HHV (MJ/kg)	18.73; 23.79
Carbon (wt%)	45.0; 56.89
Hydrogen (wt%)	7.50; 6.55
Oxygen (wt%)[b]	47.50; 36.56
Nitrogen (wt%)	< 0.2; < 0.2

Sulfur below de detection limit.
[a] Values are the average of two measurements.
[b] Determined according to Eq. (1).

Consequently, the results from SCB fast pyrolysis are outside the typically observed tendency that higher ash content in the feedstock lowers organic liquid yield [51,52]. This observation can be explained with the low potassium content in the feedstock. Most inorganics are due to silicium which can be regarded inert for pyrolysis. Sulfur was below de detection limit, which is in accordance with the low concentration in the SCB previously presented in Section 3.1.

The SCBPO exhibits comparably high water content given the gas temperature of around 90 °C after the first condensation step. This observation is attributed to the cooling water temperature of 30 °C in the first condenser of the SCBPO sampling train which potentially leads to condensate temperatures < 90 °C at the tube's wall and thus increased condensation of water vapor. However, this fact has limited effects on subsequent hydrotreatment.

The SCBPO was deeply characterized in terms of chemical composition by GC–MS/FID as well as by GC/MS and later discussed (see Fig. 5 and Fig. 6 Section 3.3.3). Its composition is in line with the low amount of lignin in the feedstock as indicated by the results from the Py-GC/MS (see Table 2), i.e. there is a slightly higher amount of sugar derivatives and lower amount of lignin derived dimethoxyphenols as typically observed for woody feedstocks.

3.3. Hydrotreatment reactions and products characterization

3.3.1. Physicochemical properties and mass balance

The upgrading reactions with the Ni/SiO_2 catalyst for the SCBPO resulted in four main phases: gas phase, solid phase, upgraded light phase (ULP) and upgraded oil phase (UOP) as the main product

Table 4
Product yields and physicochemical properties of upgraded liquid products.

Mass balance	Ni/SiO_2	Ni-Cr/SiO_2
Upgraded oil phase UOP (wt%)	55.79	24.71
Intermediate upgraded phase IUP (wt%)	–	21.12
Upgraded light phase ULP (wt%)	29.99	35.56
Solid (wt%)	0.24	1.14
Gas (wt%)	5.24	7.12
Loss (wt%)	8.73	10.36
DOD (%)[a]	$43.3^{(UOP)}$	$38.0^{(IUP)}$;$32.2^{(UOP)}$

Size exclusion chromatography	SCBPO	$UOP_{Ni/SiO2}$	$IUP_{Ni-Cr/SiO2}$	$UOP_{Ni-Cr/SiO2}$
Mn (g/mol)	177.9	248.8	226.6	235.21
Mw (g/mol)	257.9	419.2	381.9	431.76
Polydispersity (Mw/Mn)	1.4	1.7	1.7	1.8

Physicochemical properties and elemental analysis (wet basis; dry basis)[c]

	$ULP_{Ni/SiO2}$	$UOP_{Ni/SiO2}$	$ULP_{Ni-Cr/SiO2}$	$IUP_{Ni-Cr/SiO2}$	$UOP_{Ni-Cr/SiO2}$
H_2O (wt%)	71.2	8.3	68.4	8.8	8.6
pH value	2.6	–	3.0	3.8	–
HHV (MJ/kg)	–	30.17; 31.89	–	29.04; 31.73	26.32; 30.42
Carbon (wt%)	13.1; 45.48	65.2; 71.1	15.2; 48.1	62.3; 68.31	60.9; 66.63
Hydrogen (wt%)	10.2; 7.94	8.1; 7.83	10.2; 8.23	8.9; 8.69	8.5; 8.25
Oxygen (wt%)[b]	76.5; 45.87	26.4; 20.74	74.4; 43.0	28.5; 22.67	30.30; 24.79
Nitrogen (wt%)	< 0.2; < 0.2	0.3; 0.33	0.2; 0.63	0.3;0.33	0.3; 0.33

[a] DOD (degree of deoxygenation) determined in dry basis as follow: $DOD\ (\%) = (1 - (O_{UOP}/O_{SCBO})) \cdot 100$.
[b] Determined according to Eq. (1).
[c] Values are the average of two measurements.

(55.79 wt%). A photograph of both liquid upgraded fractions is available (Fig. S.1d). A different product composition was observed after hydrotreatment with Ni-Cr/SiO_2. The upgrading step also resulted in gas, solid, ULP and UOP but an additional intermediate upgraded phase was observed (Table 4). This extra phase is denoted IUP, considering that after centrifugation (see Section 2.3) this additional phase was concentrated between the heavy (UOP) and the light phase (ULP). The IUP was visibly less viscous compared to the UOP (paste-like upgraded product). The main product obtained with Ni-Cr/SiO_2 was the ULP, corresponding to 35.56 wt%. Higher amounts of solid were also obtained with Ni-Cr/SiO_2, almost 5 times higher compared to the amount generated with Ni/SiO_2. The losses for both catalysts were around 9.5 wt%, possibly due to the difficulty to completely recover the upgraded products from the autoclave, as previously reported [44].

For the viscosity measurements, the SCBPO, $UOP_{Ni/SiO2}$ and $IUP_{Ni-Cr/SiO2}$ were analyzed (Fig. S.4). Due to the low sample amount and the priority given to another analytical techniques, it was not possible to analyse the $UOP_{Ni-Cr/SiO2}$. The SCBPO and the upgraded products showed a non-Newtonian behavior (shear thinning) as previously observed in other studies [69]. Additionally, an increase of viscosity after hydrotreatment was observed for both upgraded products analyzed in comparison to SCBPO, with highest viscosity observed in this case for $UOP_{Ni/SiO2}$. Although not analyzed, the $UOP_{Ni-Cr/SiO2}$ had a paste-like consistency, which most probably indicates a higher viscosity when compared to the SCBPO and the highest viscosity among the upgraded products presented here. Hydrotreatment has been usually suggested as a step for polymerization elimination [70], reducing the pyrolysis oil viscosity, as previously reported elsewhere [71]. Jahromi et al. [30] observed that the lower viscosity values were obtained with nickel-based catalysts with higher nickel loading. These finds are the opposite of our observations for SCBPO, even with the high loaded nickel catalyst (Ni-Cr/SiO_2). In our specific case, the behavior of SCBPO under hydrotreatment condition was different from previous observations for beech wood FPBO, which visually showed lower viscosity after upgrading [29,44]. In the previous study, we assumed that the stabilization step of FPBO took place during the heating ramp [57,72]. The stabilization is usually suggested in order to reduce reactivity and to avoid excessive char production and polymerization and is performed at mild temperature conditions [73,74]. However, in the present study on SCBPO it seems that the stabilization during the heating ramp is not enough to avoid polymerization which competed with hydrotreating reactions. Differences in composition among the beech wood and SCB bio-oil may explain the difference in the products obtained from upgrading. In order to unravel whether in fact polymerization reactions occur during the upgrading, the molecular weight distribution was measured by size exclusion chromatography (Table 4). The measurements were conducted with SCBPO, $UOP_{Ni/SiO2}$, $IUP_{Ni-Cr/SiO2}$ and $UOP_{Ni-Cr/SiO2}$. SEC plots are available in the Supplementary Material (Fig. S.6).

A closer look was given to the molecular weight tail, which provides information regarding polymerization [75,76]. The upgraded products caused higher intensity in higher molecular weight ranges when compared to the un-treated SCBPO. These observations are in agreement with the Mn and Mw from SEC given in Table 4. Although interaction of different chemical groups present in the sample may also influence the retention times during the SEC measurement [77], the Mn and Mw number were used as a rough indication of polymerization reactions taking place during the hydrotreatment, especially in the case of the $UOP_{Ni-Cr/SiO2}$. The SEC results are in agreement with the viscosity. Therefore, the upgraded products with higher viscosity show the higher molecular weight.

A reduction of around 60.3% of the water content was observed in the UOP applying the Ni/SiO_2 catalyst in comparison to SCBPO. In the case of Ni-Cr/SiO_2, an IUP with 57.9% less water in comparison to the feed was obtained, whereas the UOP showed 58.8% less water compared to the feed. The highest degree of deoxygenation (DOD) was obtained with Ni/SiO_2, resulting in a reduction of the oxygen content of around 43.3%. In the case of the products obtained with Ni-Cr/SiO_2, a

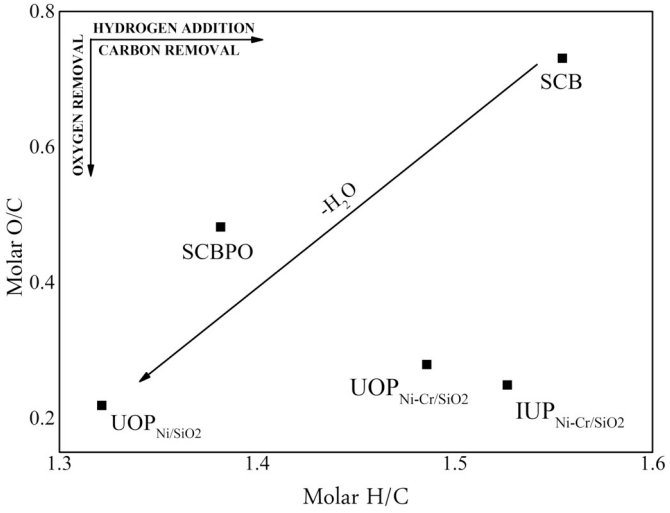

Fig. 3. Van Krevelen diagram of sugarcane bagasse, fast pyrolysis bio-oil (dry basis) and upgraded products (dry basis).

higher DOD was observed for the IUP (38.0%), compared to the UOP (32.2%). In total, 2.52 g of H_2O were formed with Ni/SiO_2, whereas 3.66 g of H_2O were formed with $Ni\text{-}Cr/SiO_2$. Although higher water formation with $Ni\text{-}Cr/SiO_2$ (35.5% extra H_2O formed in total) in comparison to Ni/SiO_2 (24.4% extra H_2O formed in total), the lowest O/C ratios in the Van Krevelen plot (Fig. 3) as well as the highest DOD were observed for the second catalyst. Two hypotheses can be raised regarding the high water formation: usually char formation due to polymerization leads to water production [21]. Hence, as the highest solid formation was observed for $Ni\text{-}Cr/SiO_2$ (later discussed in Section 3.3.4), it can be expected that also the highest water formation occurs. Secondly, the presence of oxides (NiO and Cr_2O_3) in the catalyst composition can lead to water formation due to the reduction of the oxide over H_2 atmosphere. In this case a maximum of approximately 0.26 g of water would be obtained, if the reduction of both NiO and Cr_2O_3, would take place. Consequently, the water formation does not reflect in the UOP's deoxygenation.

Most of the carbon was recovered in the UOP obtained with both catalysts and in the $IUP_{Ni\text{-}Cr/SiO2}$.Considering the carbon initially present in the FBPO, 80.8% was recovered in the UOP with Ni/SiO_2, whereas 62.7% was recovered with $Ni\text{-}Cr/SiO_2$ in the organic rich fractions (sum of 33.45% of carbon recovered in the $UO_{Ni\text{-}Cr/SiO2}$ and 29.3% in the $IUP_{Ni\text{-}Cr/SiO2}$) after the upgrading. An overall recovery from SCB to upgraded oil phase of 41.9% was obtained with Ni/SiO_2 and 32.5% with $Ni\text{-}Cr/SiO_2$ (sum of 17.3% recovered in the UOP and 15.2% recovered in the IUP).

Nitrogen was observed in low concentration in all upgraded liquid product phases, whereas sulfur was not observed in the upgraded products, which is in agreement with the low sulfur content in SCB as well as the absence of sulfur in the SCBPO, as reported in Section 3.1 and Section 3.2. In addition to the lowest water and oxygen content of the UOP obtained with Ni/SiO_2, the reaction also resulted in the upgraded product with the highest carbon content (71.1 wt%). As a consequence, the HHV for this fraction was slightly higher (31.89 MJ/kg) compared to the value obtained to the IUP (31.73 MJ/kg) and the UOP (30.42 MJ/kg), both obtained with $Ni\text{-}Cr/SiO_2$ catalyst. In all cases, the HHV increased significantly in comparison to the feed (23.79 MJ/kg_{SCBPO}, dry basis).

The Van Krevelen diagram considering the upgraded fractions (light phases are not included), as well as SCB and SCBPO is shown in Fig. 3. The O/C ratio is significantly reduced in the SCBPO in comparison to SCB. A clear reduction of O/C ratio after hydrotreatment reactions is observed with both catalysts, especially with Ni/SiO_2 (0.22). The H/C ratio is reduced after the fast-pyrolysis step (1.55 to SCB and 1.38 to SCBPO), as well as in the UOP obtained with Ni/SiO_2, indicating hydrodeoxygenation [21] and dehydration due to polymerization [78]. It is in agreement with the DOD results previously discussed. Upgraded products obtained with $Ni\text{-}Cr/SiO_2$ showed higher values of H/C ratios. It indicates high hydrogenation activity [79] and agrees with the highest hydrogen consumption (Table 5) observed for reactions conducted with this catalyst.

Table 5
Hydrogen consumption and chemical composition of the gas fraction.

	Ni/SiO_2	$Ni\text{-}Cr/SiO_2$
Hydrogen consumption (NL/Kg feed)	199.43	326.2
Gas composition		
Carbon dioxide (mol/kg feed)	1.146	1.263
Carbon monoxide (mol/kg feed)	0.041	0.058
Methane (mol/kg feed)	0.016	0.718
Propane (mol/kg feed)	[a]	0.015
Ethane (mol/kg feed)	0.007	0.045
n-butane (mol/kg feed)	[a]	0.007

[a] Values below the limit of quantification.

3.3.2. Gas fraction characterization: consumption of hydrogen and chemical composition

The gas composition was taken into account in order to investigate the main products as well as the H_2 consumption. Experiments with $Ni\text{-}Cr/SiO_2$ showed the highest consumption of hydrogen (Table 5) and also the highest gas production (7.12 wt%) compared to Ni/SiO_2 (5.24 wt%). For both catalysts, carbon dioxide was the main product, followed by carbon monoxide and methane. Smaller amounts of C2–C4 compounds were also detected. Similar to our previous findings with $NiCu/SiO_2$ catalysts [29], high hydrocracking activity was observed for the catalyst which consumed the highest amount of hydrogen, leading higher methane formation [30,80], possibly resulting in excessive consumption of hydrogen during this step [81].

The internal pressure and temperature of the autoclave were recorded along the reaction (Fig. 4). The catalysts showed different pressure profiles. While the pressure profile for Ni/SiO_2 increased close to linearity during the heating ramp (even with consumption of hydrogen taking place), more pronounced hydrogen consumption was observed for $Ni\text{-}Cr/SiO_2$. A rough trend was plotted using the ideal gas and Soave Redlich Kwong equations to estimate the theoretical H_2 pressure in the autoclave without gas consumption. After 20 min of reaction at 97.7 °C with Ni/SiO_2, the recorded autoclave pressure is lower compared to the theoretical values, which gives an indication of H_2 consumption started already at lower temperatures [72,74]. Even if gaseous compounds are formed during this step (neglected in this approach), the H_2 consumption is still visible, considering the distance from the theoretical plots. At 50 min of reaction (159 bar and 257.5 °C) the pressure recorded is higher compared to the theoretical plots. It can be attributed to cracking reactions, mostly occurring at higher HDO temperatures [44,82], resulting mainly in decarboxylation [73], considering that CO_2 is the main gaseous product (Table 5). At 324.3 °C (approximately 77 min of reaction) the reaction with Ni/SiO_2 reached the highest pressure recorded for this catalyst (202.6 bar). A slightly decreased was observed after this point, reaching 194.4 bar (measured at 324.9 °C) at the end of the reaction (indication of H_2 consumption).

The hydrogen consumption profile with $Ni\text{-}Cr/SiO_2$ was more pronounced compared to Ni/SiO_2, in agreement with Table 5. After 22 min of reaction time, the reactor reached 88.8 °C and 104.3 bar. The pressure then decreased to approximately 95.6 bar, remaining at this range for about 9 min (temperature from 143.5 °C to 189 °C). A second pronounced pressure decrease is observed as the temperature continues to rise; a new plateau was observed at approximately 85.7 bar from 219.2 °C to 270.5 °C. After 57.4 min of reaction a sharp pressure increase could be noticed, reaching 140.1 bar (324.2 °C) in approximately

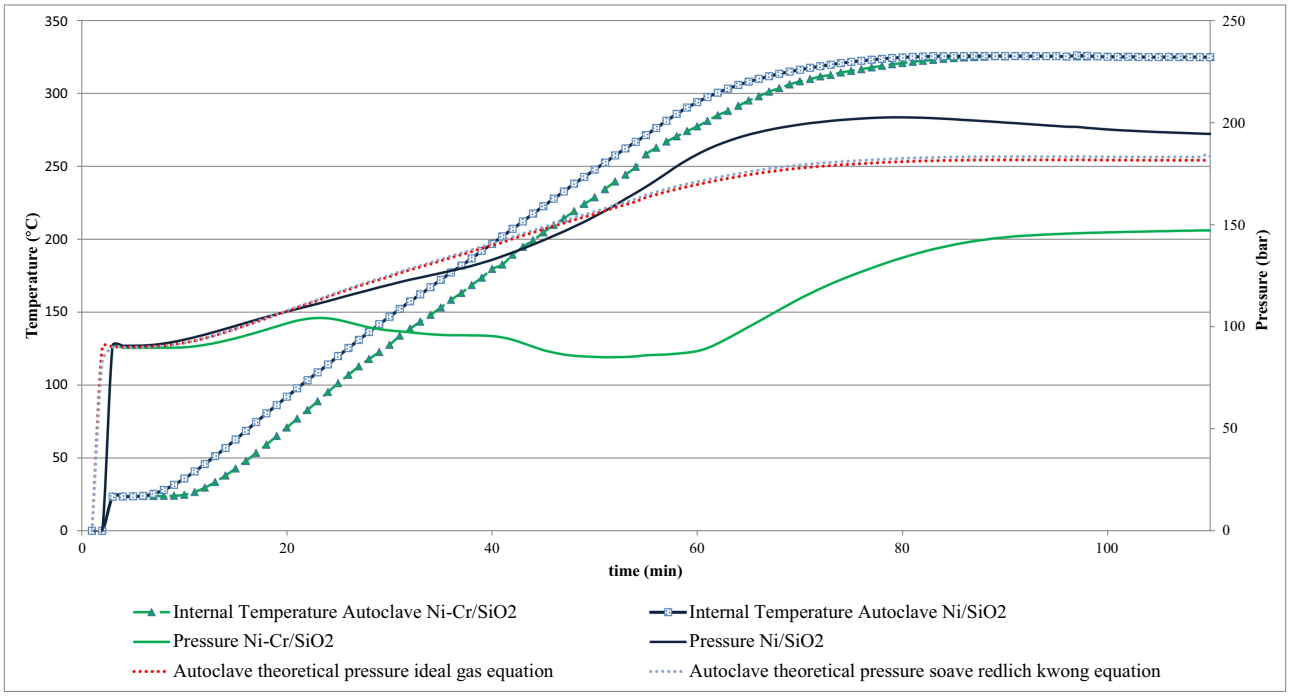

Fig. 4. Pressure and temperature registered during the upgrading reactions as well as the theoretical hydrogen pressure expected if no consumption of H_2 would occur. Ideal gas equation and Soave Redlich Kwong equation were used for the theoretical calculation.

26 min (rate of 1 bar/°C), similar to the behaviour observed to Ni/SiO_2. After reaching the set point (325 °C), the pressure remained in the range of 146 bar. The highest pressure of 147.8 bar was recorded at the end of the reaction with $Ni\text{-}Cr/SiO_2$ (46.6 bar below Ni/SiO_2). It is an indication of higher catalytic activity and higher hydrogen consumption [72].

Based on the pressure profiles obtained for both catalysts, H_2-TPR result (Fig. S.6) and our previous investigation of the influence of temperature (175 °C, 225 °C, 275 °C and 325 °C) on the conversion of a beech wood FPBO [44], some conclusions can be derived (further discussed in Section 3.3.4). The H_2-TPR of $Ni\text{-}Cr/SiO_2$ (Supplementary material Fig. S.6), showed very little H_2 consumption and H_2O production, starting mostly at around 83 °C and reaching the maximum H_2 consumption at 210 °C. This observation could partly explain the H_2 consumption behavior during the upgrading reaction (reduction of oxides). In the sequence, the H_2 consumption and water production are reduced during the TPR measurement, although some H_2 is still being consumed in even lower amounts. In the case of the upgrading reactions, the hydrogen consumption takes already place at low temperatures, around 88.8 °C with $Ni\text{-}Cr/SiO_2$ and around 97.7 °C with Ni/SiO_2, might be an indication of hydrogenation of reactive compounds such as olefins, aldehydes and ketones, as these compounds are usually the first to be hydrogenated [11,57,83]. Furthermore, the low hydrogen uptake temperatures observed in both cases, but especially for $Ni\text{-}Cr/SiO_2$, are in agreement with the observations of Yin et al. [45]; the authors observed an H_2 uptake at around 80 °C, also using a high loaded Ni-based catalyst ($NiCu/SiO_2$). Mercader et al. 2011 [74] also reported hydrogen consumption taking place at this temperature. The plateaus observed at different temperature ranges for $Ni\text{-}Cr/SiO_2$ could be correlated to the reactivity range of some bio-oil components [83]. While very reactive compounds react at lower temperature, compounds with intermediate reactivity react mainly in the second plateau (219.2 °C to 270.5 °C). For example, Boscagli [57] observed that some ketones can be formed at slightly higher temperature ranges, whereas according to Elliott [83] some aliphatic alcohols can undergo thermal dehydration at moderate temperatures forming olefins (in our case olefins were only observed in the UOP with $Ni\text{-}Cr/SiO_2$ and later discussed at Section 3.3.4). Hydrocracking and decarboxylation can be a plausible explanation for the sharp pressure increase with both catalysts at very similar temperatures (257.5 °C and 270.5 °C), as C2–C3 gaseous compounds, methane and carbon dioxide concentration are directly related to the increase of the reaction temperature [44,57].

3.3.3. Chemical composition of sugarcane bagasse fast pyrolysis bio-oil and upgraded liquid fractions

In the following, the main chemical transformations which took place during the upgrading reactions of SCBPO in terms of GC detectable fraction are described. Usually around 20–40% of all the compounds can be identified by gas chromatography [84,85]. Additionally, the Py-GC results of SCB and the main constituents of the SCBPO are correlated and discussed in comparison to the upgraded products. The compounds identified by GC–MS/FID are grouped and presented in Fig. 6, whereas the detailed quantification of single compounds is given in Table S.4 together with the GC/MS measurements (Fig. S.3 and Table S.3).

The main chemical compounds observed in the SCBPO (Table S.4) are in agreement with the Py-GC measurements with SCB (Table 2). In total, 28 compounds obtained by this analytical technique (from a total of 71) are observed in the SCBPO. In both cases, acetic acid, hydroxyacetaldehyde, hydroxypropanone and levoglucosan are observed as the main pyrolysis products, as well as furfural, 2(5H)furanone, 3-hydroxypropanal. In minor concentration, 9 of the 10 compounds belonging to the guaiacol group were observed in both cases. Some lignin derived phenols (phenol, p-cresol and m-cresol) and some of syringol's group belonging compounds (syringol, 4-methylsyringol, 4-vinylsyringol and syringaldehyde) were also obtained as products from the analytical and technical scale pyrolysis. All the sugars identified in the SCBPO pyrolysis experiment were in agreement with this analytical technique. Due to the operational differences between both methods, as residence time and temperature, different fragmentation products are expected [62] and in fact observed. The main pyrolysis products and the precursor building blocks are highlighted in Fig. 5, in brown and black color, respectively.

In terms of the upgraded products, the ULPs concentrated most of the water and most of the nonaromatic compounds (Fig. 6). Considering

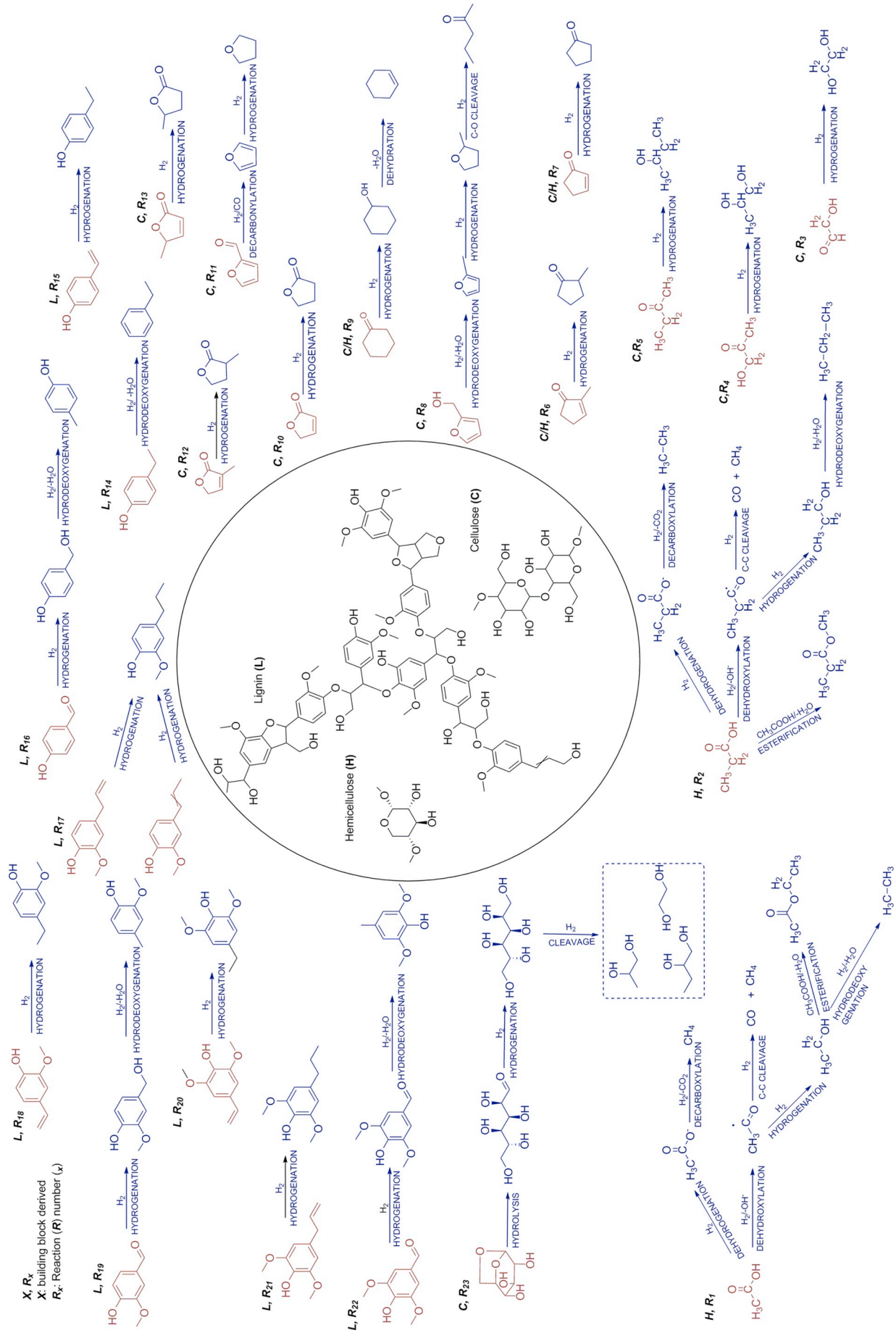

Fig. 5. Some of the main SCB pyrolysis products are depicted (brown color) and some of the reaction pathways observed during the upgrading treatment (blue color).The building blocks of SCB are represented in black color (hemicellulose represented by α-D-Xylopyranose). Esterification reactions in H, R_1 and H, R_2, and the pathways from cyclohexanol to cyclohexene in C/H R_9 are mostly observed for Ni-Cr/SiO_2 catalyst. The molecules are identified with regard to the main source from which are derived (H: hemicellulose; C: cellulose and L: lignin) as well as by the reaction (R) number. (For interpretation of the references to color in this figure legend, the reader is referred to the web version of this article.)

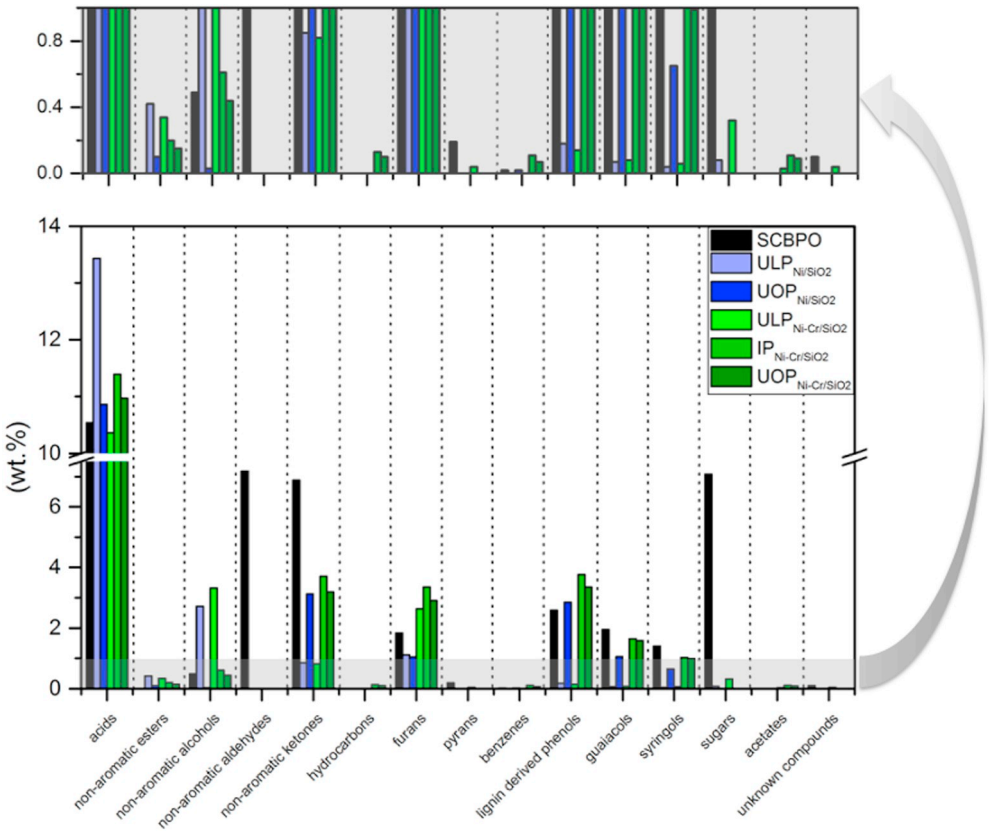

Fig. 6. Distribution of the main chemical compounds in the SCBPO and upgraded products.

the concentration on dry basis, the $ULP_{Ni/SiO2}$ was composed by 63.88 wt% of nonaromatic compounds (sum of acids, non-aromatic alcohols, non-aromatic aldehydes, non-aromatic ketones, and hydrocarbons), whereas the $ULP_{Ni-Cr/SiO2}$ was composed by 48.85 wt% of nonaromatic compounds. Among the nonaromatics in the ULPs, organic acids contributed to 49.24 wt% of ULP $_{Ni/SiO2}$ and 34.11 wt% of $ULP_{Ni-Cr/SiO2}$, reflecting the lower pH value [86] observed (Table 4). The lowest pH was observed for the reaction with Ni/SO_2 (pH value 2.6), the fraction with highest concentrations of acetic acid. On the other hand, UOPs with both catalysts as well as the $IUP_{Ni-Cr/SiO2}$ showed similar concentration of organic acids (around 12.30 wt%), mainly acetic and propionic acid. Initially, the feed contained 3.35 g of acetic acid while the liquid products showed lower amounts (calculated as the sum of acetic acid in the liquid upgraded fractions). The conversion with Ni/SiO_2 resulted in 3.10 g of acetic acid in the products while reactions performed with $Ni-Cr/SiO_2$ resulted in 2.49 g of acetic acid in the upgraded products. Considering the initial concentration, 7.5% of the acetic acid was converted with Ni/SiO_2, while 25.7% was converted by $Ni-Cr/SiO_2$. The conversion was calculated considering the initial moles of acetic acid in the SCBPO and the sum of moles of acetic acid in the upgraded liquid products. The possibility of acetic acid formation, for example, as a byproduct from levoglucosan scission [60,61] was not considered in this case. Acetic acid, mainly formed from depolymerization of hemicellulose [36,87], and as just previously mentioned from levoglucosan, can follow different reaction pathways during the bio-oil upgrading (Fig. 5 H, R_1). It can be converted to CH_4 and CO_2 by deprotonation to acetate followed by decarboxylation to methane [88]. After dehydroxylating to acetyl species followed by C—C bond cleavage results in CO and CH_4 [89]. The lower concentration of acetic acid and higher production of CH_4 observed with $Ni-Cr/SiO_2$ could be correlated to the methane formation pathway (higher methane concentration observed with this catalyst). Additionally, the acetyl species can undergo hydrogenation to ethanol (not detected), which can be further hydrodeoxygenated to ethane or follow esterification to ethylacetate [73,89], both identified in the products.

Propionic acid, derived from hemicellulose pyrolysis [63,88], was observed in the SCPBO, as well as in the upgraded products. Considering the initial loading of SCBPO (around 50 g) and the concentration of propionic acid (3.73 wt%), 1.84 g of propionic acid was loaded in the batch reactor. After the upgrading reaction a total of 1.81 g and 1.56 g of propionic acid were observed in the upgraded products with Ni/SiO_2 and $Ni-Cr/SiO_2$, respectively. Lower conversion (1.56%) was observed with Ni/SiO_2 in comparison to $Ni-Cr/SiO_2$ (14.95% of conversion). Propionic acid can be converted (i) to ethane through dehydrogenation followed by decarboxylation [90], can (ii) undergo dehydroxylation and hydrogenation resulting in 1-propanol [91], identified mainly in the products with $Ni-Cr/SiO_2$, and can (iii) also undergo esterification, resulting in products such as propanoic acid, methyl ester, observed in the products [78] and shown in Fig. 5 H, R_2. Similarly to acetic acid, propionic acid can also be decomposed to CH_4 [91], which could be another explanation for the higher concentration of methane (Table 5) observed with $Ni-Cr/SiO_2$.

Butyric acid and pentanoic acid, initially absent in the SCPBO, were observed in the products, mainly in the ULP obtained with Ni/SiO_2 and in all the products obtained with $Ni-Cr/SiO_2$ (pentanoic acid is not observed in the UOP with $Ni-Cr/SiO_2$). Although observed in lower concentration compared to acetic and propionic acids, the high concentration of these acids in the upgraded oils are in agreement with other studies [92,93] and can be considered a limitation for further applications, due to UOP's corrosiveness and catalytic effect on oligomeric sugars, which can result in solids formation [94].

Nonaromatic esters were observed in both phases obtained with Ni/SiO_2 (Fig. 6), but with higher concentration found in the $ULP_{Ni/SiO2}$ (1.55 wt% dry basis), followed by $UOP_{Ni/SiO2}$ (0.11 wt% dry basis). The upgraded products with $Ni-Cr/SiO_2$ also showed nonaromatic esters in all three phases. The highest concentration was observed in the ULP_{Ni-}

$_{Cr/SiO2}$ (1.12 wt% dry basis), followed by $IUP_{Ni\text{-}Cr/SiO2}$ (0.22 wt% dry basis) and lower concentrations in the $UOP_{Ni\text{-}Cr/SiO2}$ (0.17 wt% dry basis), although higher compared to $UOP_{Ni/SiO2}$ (0.11 wt% dry basis). The esterification has been proposed to reduce the acidity of the pyrolysis oils [95]. Propanoic methyl ester was observed in the upgraded products with both catalysts, whereas acetic acid butyl ester was just detected in the products obtained with Ni-Cr/SiO_2. Acetic acid 2-hydroxyethyl ester was only observed in both $ULP_{Ni\text{-}Cr/SiO2}$ and $ULP_{Ni/SiO2}$ ULPs, while propanoic acid, 2-hydroxyethyl was exclusively observed in the $ULP_{Ni/SiO2}$.

In terms of non-aromatic alcohols, higher concentrations were observed in the ULP with both catalysts in comparison to the feedstock (Fig. 6). Ethylenglycol was the only compound initially found in the SCBPO (0.49 wt% dry basis), considering its application as start-up material mentioned in Section 2.2. The reaction with Ni/SiO_2 resulted in an increased absolute ethyleneglycol content (0.24 g in the feed versus 0.41 g after reaction as sum of LP + HP), mainly concentrated in the ULP. A small concentration of 1-propanol was also observed in the ULP, as already discussed, whereas an unknown aliphatic alcohol was observed in the UOP. The reaction performed with Ni-Cr/SiO_2 followed a different pathway: 9 non-aromatic alcohols were identified in the ULP (Table S.4). Ethyleneglycol was the main alcohol (6.42 wt% dry basis, 0.34 g), followed by propyleneglycol (2.48 wt% dry basis) and 1-propanol (1.06 wt% dry basis). Other compounds were present in the ULP in smaller concentrations. 1-propanol and 2-methyl-1-propanol were observed in the IUP, whereas 1-propanol was only identified in the UOP. The high concentration of ethyleneglycol in the products in comparison to the feed can be related to the complete hydrogenation of hydroxyacetaldehyde (Fig. 5 C, R_3), the non-aromatic aldehyde initially present in the SCBPO in higher concentration (6.03 wt% wet basis) [96]. Following the same pathway, propylene glycol most probably was formed by the hydrogenation of acetol (Fig. 5 C, R_4) [29,96,97]. Initially present in high concentration in the SCBPO (6.20 wt% dry basis, 2.44 g in total), it was mostly converted after the upgrading reactions, remaining only 0.04 g in the ULP. Ni-Cr/SiO_2 seems to favor the hydrogenation, considering that propylene glycol was the second most abundant alcohol in the ULP with this catalyst, whereas the upgrading with Ni/SiO_2 followed a different pathway, as no propylene glycol was observed in none of the fractions obtained with this catalyst. Additionally, alcohols such as 2-butanol observed in the $ULP_{Ni\text{-}Cr/SiO2}$ can be a product of 2-butanone hydrogenation (Fig. 5 C, R_5) [11]. In the same way, alcohols in smaller concentration, such as cyclohexanol, is a product of cyclohexanone hydrogenation.

Initially 12 ketones were identified in the SCBPO, with acetol as the main compound. In total, the SCBPO was composed by 8.65 wt% (3.40 g) of ketones (Fig. 6). Other compounds belonging to the ketone group, mostly unsaturated cyclic compounds, were in much lower concentration. In the same way as observed for acetol, which was most hydrogenated to propylenglycol [98], most of the compounds initially present were hydrogenated. For example, 2-methyl-2-cyclopenten-1-one was possibly hydrogenated to 2-methyl-cyclopentanone (Fig. 5 C/H, R_6), and 2-cyclopenten-1-one possibly hydrogenated to cyclopentanone (Fig. 5 C–H, R_7) [93]. On the other hand, ketones such as 2-pentanone, initially absent in the SCBPO were identified in the products. It can be explained by the hydrodeoxygenation of 2-furfurylalcohol to 2-methylfuran, followed by hydrogenation/C—O bond cleavage, resulting in 2-pentanone (Fig. 5 C, R_8) [88]. Additionally, ketones can undergo hydrogenation to alcohols and dehydration to olefins [99], as exemplified in Fig. 5 (C/H, R_9). In summary, the upgrading with Ni/SiO_2 reduced the initial total amount of ketones (3.40 g) to 0.99 g and to 0.92 g of ketones with Ni-Cr/SiO_2.

Hydrocarbons, initially absent in the SCBPO were observed only in the $IUP_{Ni\text{-}Cr/SiO2}$ (0.15 wt% dry basis) and $UOP_{Ni\text{-}Cr/SiO2}$ (0.01 wt% dry basis). The hydrocarbons identified in the IUP were cyclohexene and ethylcyclopentane in smaller concentration. Cyclohexene could be formed from the hydrogenation of cyclohexanone to cyclohexanol, followed by dehydration to cyclohexene (Fig. 5 C/H, R_9) [91]; both precursors, cyclohexanone and cyclohexanol, only observed in the upgraded products with Ni-Cr/SiO_2.

The number of molecules belonging to group of furans, products of carbohydrates depolymerization [11,63], increased after upgrading reactions (Fig. 6). Initially, 8 molecules attributed to furan group were identified in the SCBPO (2.31 wt% dry basis, corresponding to 0.91 g of furans), mainly composed by 2(5H)-furanone, 2-furaldehyde and γ-butyrolactone (Table S.4). After the upgrading reaction, a total of 10 compounds were identified in the upgraded phases with Ni/SiO_2 (resulting in 0.46 g of furans, sum of all fractions), as well as 17 compounds were identified in the products obtained with Ni-Cr/SiO_2 (1.17 g, sum of all fractions), mostly concentrated in the ULP (8.68 wt% dry basis, 0.46 g).

Compounds initially present in the feedstock, such as 2-furfuryl alcohol, 2(5H)-furanone, 3-methyl-2(5H)-furanone, 2-furaldehyde, 4-methyl-(5H)-furan-2-one and 5-methyl-2(5H)-furanone were completely converted with both catalysts. On the other hand, compounds such as γ-butyrolactone were observed in higher concentration in the products, (0.27 g in the products with Ni/SiO_2 and 0.30 g in the products with Ni-Cr/SiO_2) in comparison to the feed (0.10 g). This may be attributed to the hydrogenation of 2(5H)-furanone, initially observed in the SCBPO and completely converted, resulting in γ-butyrolactone (Fig. 5 C, R_{10}) [29,100].

Tetrahydrofuran, a molecule absent in the SCBPO, was observed in the upgraded products. The decarbonylation of furfural leads to the formation of furan which is further hydrogenated to tetrahydrofuran (Fig. 5 C, R_{11}) [101]. α-methyl-γ-butyrolactone, observed only in the upgraded products, is a product of hydrogenation of 3-methyl-2(5H)-furanone (Fig. 5 C, R_{12}). The hydrogenation of 5-methyl-2-furanone results in γ-valerolactone (Fig. 5 C, R_{13}). Tetrahydro-2-methyl-furan was observed only in the upgraded products with Ni-Cr/SiO_2. The hydrodeoxygenation of furfuryl alcohol results in 2-methylfuran which is then further hydrogenated to tetrahydro-2-methyl-furan (Fig. 5 C, R_8). A further pathway can be followed by which 2-methylfuran can be converted to 2 pentanone [101], which was identified in all upgraded liquids with both catalysts.

The GC-detectable aromatic compounds in the SCBPO as well as in the upgraded products were classified in four main groups: benzenes, lignin derived phenols, guaiacols and syringols (Fig. 6 and Table S.4). Initially, the SCBPO was composed by 7.50 wt% (dry basis) of GC detectable aromatic compounds, considering the 30 compounds identified and quantified. The upgrading reactions with Ni/SiO_2 resulted in low concentration of aromatics (1.05 wt% dry basis) in the ULP and UOP with 5.16 wt% (dry basis), respectively. Considering the initial amount of SCBPO loaded to the autoclave, 2.95 g of aromatics were reduced to 1.30 g of aromatics (1.26 g in the UOP) with Ni/SiO_2. The reactions conducted with Ni-Cr/SiO_2 resulted in 1.46 g of aromatics, mostly concentrated in the IUP (7.16 wt% dry basis, 0.68 g) and UOP (6.71 wt % dry basis, 0.73 g) with minor concentration in the ULP (0.28 wt% dry basis, 0.05 g).

Benzene was present in the SCBPO, as well as in the upgrading products. Small concentration of toluene and ethyl-benzene were obtained with Ni-Cr/SiO_2. Ethyl-benzene could be formed from hydrodeoxygenation of 4-ethylphenol molecule (Fig. 5 L, R_{14}), analogous to the reaction pathway reported by Gandarias et al., [102] to 2-ethyl-phenol.

Lignin derived compounds were observed in the feedstock as well as in the products (Fig. 6 and Table S.4). Molecules such as phenol, cresols and 4-ethyl-phenol, were mainly concentrated in the UOP (3.21 wt% dry basis, 0.786 g and 3.75 wt% dry basis, 0.41 g for Ni/SiO_2 and Ni-Cr/SiO_2,respectively) and in the $IUP_{Ni\text{-}Cr/SiO2}$ (4.12 wt% dry basis, 0.392 g). 4-Ethyl-phenol was the main lignin derived compound observed in the UOP with Ni/SiO_2 (1.83 wt% dry basis, 0.50 g) and in the IUP (2.43 wt % dry basis, 0.52 g) and UOP (2.39 wt% dry basis, 0.29 g) with Ni-Cr/SiO_2. It seems that the molecules already present in the feed (0.55 wt%,

0.27 g) were not further converted, whereas the complete hydrogenation of 4-vinyl-phenol contributed to the increased concentration of this compound in the products (Fig. 5 L, R_{15}). 4-Hydroxy-benzaldehyde was also completely converted with both catalysts. A possible pathway for its conversion could be the hydrogenation followed by hydrodeoxygenation, resulting in 4-methylphenol (p-cresol) (Fig. 5 L, R_{16}).

Most of the guaiacols initially present were converted with both catalysts. Ni/SiO_2 was able to convert the highest amount of guaiacols (feed: 0.96 g; sum of products: 0.30 g) in comparison to $Ni\text{-}Cr/SiO_2$ (feed: 0.96 g; sum of products: 0.38 g). In this case, possible products formed from depolymerization of GC non-detectable fraction are not considered. Compounds such as eugenol, isoeugenol, 4-vinylguaiacol and vanillin were completely converted with both catalysts, whereas compounds such as guaiacol, 4-methylguaiacol and 4-ethylguaiacol were in the feed and in the product, mostly concentrated in the UOPs as well as in the $IUP_{Ni\text{-}Cr/SiO2}$. In agreement with our previous findings [29,44], eugenol, cis and trans isoeugenol were completely hydrogenated most probably to 4-propylguaiacol, identified only in the products (Fig. 5 L, R_{17}). In the same way 4-vinylguaiacol was possibly completely hydrogenated to 4-ethylguaiacol (Fig. 5 L, R_{18}). The complete conversion of vanillin after the upgrading and higher concentration of 4-methylguaiacol found in the products suggests that hydrogenation followed by hydrodeoxygenation was a possible reaction pathway for the vanillin (Fig. 5 L, R_{19}) [103].

Initially 11 compounds belonging to the syringol group are present in the SCBPO. After the upgrading reactions, 8 substances were completely converted with both catalysts and mostly concentrated in the UOPs and $IUP_{Ni\text{-}Cr/SiO2.}$ Both 4-vinyl-syringol and 4-allyl-syringol were completely hydrogenated to 4-ethyl-syringol and 4-propyl-syringol, respectively (Fig. 5 L, R_{20} and L R_{21}); Syringaldehyde on the other hand, possibly underwent hydrogenation, followed by hydrodeoxygenation, resulting in 4-methyl-syringol (Fig. 5 L R_{22}).

Sugars contained in SCBPO such as levoglucosan, 1,5-anhydro-β-D-xylofuranose, and 1,5-anhydro-β-D-arabinofuranose, were completely converted. Levoglucosan, derived from the thermal degradation of cellulose [36] is considered to be converted to compounds such as ethyleneglycol, propyleneglycol and 1,2-butanediol [96,100], identified mainly in the products with $Ni\text{-}Cr/SiO_2$. Firstly levoglucosan is converted by hydrolysis to glucose [79,100], which is hydrogenated to sorbitol [102,104], and later undergoes hydrogenolysis to diols as observed in the products (Fig. 5 L, R_{20} and C R_{23}) [102,105]. As previously stated, acetic acid is also one possible product from levoglucosan scission [60,61]. Sugars are also known for polymerization during the hydrotreatment reactions, leading the formation of char and carbon dioxide [105]. This pathway cannot be discarded, considering the char deposition observed over the spent catalysts (later discussed in Section 3.3.4). Furthermore, gaseous products such as ethane and methane might be also generated from sugars conversion [72]. A small amount of unknown sugars was observed in the ULPs, as well as a small concentration of isosorbide in the $ULP_{Ni\text{-}Cr/SiO2}$.

Acetates were mostly observed in the upgraded liquid products obtained with $Ni\text{-}Cr/SiO_2$, mainly composed by tetrahydro-2-furanmethanol acetate and ethylacetate, respectively. Tetrahydro-2-furanmethanol acetate is formed from the esterification reaction of acetic acid and a furfural intermediate [98,106]. The reaction of carboxylic acids and 2-furanmethanol and derivatives, can result in a less corrosive and more stable pyrolysis oil [101]. Minor unknown compounds were observed in the samples as well.

3.3.4. Catalysts characterization

The catalysts were characterized before and after the upgrading reaction. Additionally, the ULP were analyzed for the amount of leached metal ions. The $ULP_{Ni\text{-}Cr/SiO2}$ showed 0.0047 wt% of Ni and concentration of Cr below the detection limit (< 0.0016 wt%). In terms of the amount of catalyst loaded to the autoclave, 0.054 wt% of the initial concentration of Ni and < 0.09 wt% of Cr were leached in the ULP, respectively. Ni (0.032 wt%) and Cr (< 0.0016 wt%) were also identified in the $IUP_{Ni\text{-}Cr/SiO2}$, which accounts 0.22 wt% of Ni and < 0.09 wt % of Cr in the $IUP_{Ni\text{-}Cr/SiO2}$. The concentration of Ni (1.05 wt%) and Cr (0.34 wt%) in the $UOP_{Ni\text{-}Cr/SiO2}$ were also analyzed, but these results cannot be considered leaching; due to the high viscosity of the $UOP_{Ni\text{-}Cr/SiO2}$, a complete separation of catalyst even after centrifugation was not possible. Similar difficulties were previously reported elsewhere [72]. So, the results presented here are most probably attributed to the catalyst particles dispersed in the $UOP_{Ni\text{-}Cr/SiO2}$. Hence, 10% of catalyst initially loaded to the autoclave (initial load of 2.49 g) remained in the $UOP_{Ni\text{-}Cr/SiO2}$, which implies that the separation of catalyst from the reaction products has to be improved in future work. The upgraded fractions obtained with Ni/SiO_2 showed 0.01 wt% and 0.014 wt% of Ni in the $ULP_{Ni/SiO2}$ and $UOP_{Ni/SiO2}$, respectively. In this case, 0.73 wt% of Ni was leached to the $ULP_{Ni/SiO2}$ (considering the 2.56 g Ni/SiO_2 with [Ni] = 7.9 wt% loaded to the autoclave). In the same way as discussed above, the complete separation of upgraded oil and the catalyst was difficult due to the high viscosity of $UOP_{Ni/SiO2}$.

In terms of carbon deposition, $Ni\text{-}Cr/SiO_2$ showed 18.5 wt% of carbon whereas Ni/SiO_2 showed 0.36 wt% of carbon after the upgrading reactions. Carbonaceous deposition can be formed due to a variety of polymerization reactions [45] caused but not limited to compounds such as sugars [105], furans and phenolic oligomers (pyrolytic lignin) [107,108]. Usually considered to be one of the main reasons for catalyst deactivation in hydrotreatment reactions [23,56], solids formation should be minimized. The higher carbon deposition observed to $Ni\text{-}Cr/SiO_2$ could be interlinked to the high metal loading, as previously reported [109], although some studies describe the opposite behavior [30].

The XRD of fresh and spent Ni/SiO_2 show similar patterns. The reflections of metallic Ni are observed in both cases, at 44.49°, 51.85°, 76.38°, 92.93° and 98.44° (Fig. S.5, Supplementary Material) [29]. The $Ni\text{-}Cr/SiO_2$ show the same reflections attributed to metallic nickel and additionally reflections attributed to NiO (37.2°, 42.6° and 62.8°). After the reaction, the NiO reflections disappeared, due to the reduction into metallic nickel under H_2 atmosphere. No reflections for Cr_2O_3 were observed for this catalyst (amorphous or dispersed chromium phase).

No significant differences in the crystallite sizes of Ni/SiO_2 are observed between the fresh and spent catalyst (in both cases a value of 17.7 nm). On the other hand the crystallite size of $Ni\text{-}Cr/SiO_2$ increased from 4.4 nm to 38.2 nm after the reaction. In another investigation, we observed an increase of the crystallite size to around 18 nm [44] with beech wood bio-oil. Furthermore, the $Ni\text{-}Cr/SiO_2$ high metal loading and medium surface area facilitates de migration of the metal particles resulting in sintering. In future, the catalyst may be pre-conditioned to receive a medium Ni particle size.

4. Conclusion

A holistic study from sugarcane bagasse characterization to upgraded products after hydrotreatment was presented. The low moisture content of 2.80 wt% and low potassium content of 0.08 wt% were reflected in the high yield of organic liquids (60.1 wt%) obtained by fast-pyrolysis, outside the range expected for residual biomass. Hydrotreatment reactions resulted in upgraded oils with lower oxygen, lower water and higher carbon content in comparison to SCBPO. Nonetheless distinct selectivities among both catalysts were observed. Ni/SiO_2 showed the highest activity for deoxygenation, reaching 43.3% of oxygen removed, as well as the highest activity for conversion of aromatics. $Ni\text{-}Cr/SiO_2$ on the other hand, revealed high hydrogenation activity and highest conversion of carboxylic acids, reaching conversions of 25.7% of acetic acid and 14.95% of propionic acid. Furthermore highest formation of alcohols and furans was observed with this catalyst. Around 41.9% of the carbon content of sugarcane bagasse was recovered in the upgraded oil obtained with Ni/SiO_2 whereas 32.5% was recovered $Ni\text{-}Cr/SiO_2$ (sum of upgraded oil and

upgraded intermediate phase). Polymerization of upgraded fractions took place with both catalysts.

In general, sugarcane bagasse proved to be an attractive feedstock for 2G biorefineries, with an overall yield of 30.5 wt% of upgraded oil. By the selection of the appropriate catalyst, the final composition of the upgraded oil can be adjusted. However, further studies should consider the minimization of polymerization during hydrotreatment reactions and higher deoxygenation levels should be targeted.

Abbreviations

SCB	sugarcane bagasse
SCBPO	sugarcane bagasse fast pyrolysis bio-oil
FPBO	fast pyrolysis bio-oil
ULP	upgraded light phase
IUP	Intermediate upgraded phase
UOP	upgraded oil phase
$ULP_{Ni/SiO2}$	upgraded light phase using Ni/SiO_2 catalyst
$UOP_{Ni/SiO2}$	upgraded oil phase using Ni/SiO_2 catalyst
$ULP_{Ni\text{-}Cr/SiO2}$	upgraded light phase using $Ni\text{-}Cr/SiO_2$ catalyst
$IUP_{Ni\text{-}Cr/SiO2}$	upgraded intermediate phase using $Ni\text{-}Cr/SiO_2$ catalyst
$UOP_{Ni\text{-}Cr/SiO2}$	upgraded oil phase using $Ni\text{-}Cr/SiO_2$ catalyst
DOD	degree of deoxygenation

Acknowledgements

The authors acknowledge the Bioeconomy Graduate Program – BBW Forwerts, Brazilian National Council for Science and Technology, BeMundus and Institute of Technological Research (IPT) for the financial support. The authors are grateful to Usina Iracema for the sugarcane bagasse samples and also grateful to Dr. Ana Alves and Prof. José Rodrigues from Superior de Agronomia, University of Lisbon, for the Py-GC/FID and Py-GC/MS measurements. We thank Pia Griesheimer, Petra Janke, Jessica Heinrich, Melany Frank and Armin Lautenbach for their support in sample characterization, Bernhard Hochstein for the viscosity measurements and Simon Wodarz for the H_2-TPR measurements.

Appendix A. Supplementary data

Supplementary data to this article can be found online at https://doi.org/10.1016/j.fuproc.2019.106199.

References

[1] S.M.R. Khattab, T. Watanabe, Policía Nacional Revolucionaria Objetivos del curso – taller, Bioethanol Prod. From Food Crop, Elsevier Inc, 2019, pp. 187–212, , https://doi.org/10.1016/B978-0-12-813766-6/00010-2.

[2] Conab, Acompanhamento da safra brasileira Cana-de-açúcar Monitoramento agrícola - Cana-de- açúcar, Brasília, https://www.conab.gov.br/component/k2/item/download/22956_506e8f00170422c62a452d3e319a6d6f, (2018) , Accessed date: 17 November 2018.

[3] A.R. Alcarde, Cana-de-Açúcar - Embrapa (n.d.), http://www.agencia.cnptia.embrapa.br/gestor/cana-de-acucar/arvore/CONTAG01_108_22122006154841.html , Accessed date: 17 November 2018.

[4] M.S. Buckeridge, A.P. de Souza, R.A. Arundale, K.J. Anderson-Teixeira, E. Delucia, Ethanol from sugarcane in Brazil: A "midway" strategy for increasing ethanol production while maximizing environmental benefits, GCB Bioenergy 4 (2012) 119–126, https://doi.org/10.1111/j.1757-1707.2011.01122.x.

[5] M.O.S. Dias, M.P. Cunha, C.D.F. Jesus, G.J.M. Rocha, J.G.C. Pradella, C.E.V. Rossell, R. Maciel Filho, A. Bonomi, Second generation ethanol in Brazil: can it compete with electricity production? Bioresour. Technol. 102 (2011) 8964–8971, https://doi.org/10.1016/j.biortech.2011.06.098.

[6] S. Macrelli, M. Galbe, O. Wallberg, Effects of production and market factors on ethanol profitability for an integrated first and second generation ethanol plant using the whole sugarcane as feedstock, Biotechnol. Biofuels. 7 (2014) 1–16, https://doi.org/10.1186/1754-6834-7-26.

[7] L. Canilha, A.K. Chandel, T. Suzane Dos Santos Milessi, F.A.F. Antunes, W. Luiz Da Costa Freitas, M. Das Graças Almeida Felipe, S.S. Da Silva, Bioconversion of sugarcane biomass into ethanol: an overview about composition, pretreatment methods, detoxification of hydrolysates, enzymatic saccharification, and ethanol fermentation, J. Biomed. Biotechnol. 2012 (2012), https://doi.org/10.1155/2012/989572.

[8] S. Al Arni, Comparison of slow and fast pyrolysis for converting biomass into fuel, Renew. Energy 124 (2018) 197–201, https://doi.org/10.1016/j.renene.2017.04.060.

[9] A.V. Bridgwater, Review of fast pyrolysis of biomass and product upgrading, Biomass Bioenergy 38 (2012) 68–94, https://doi.org/10.1016/j.biombioe.2011.01.048.

[10] T. Kan, V. Strezov, T.J. Evans, Lignocellulosic biomass pyrolysis: A review of product properties and effects of pyrolysis parameters, Renew. Sust. Energ. Rev. 57 (2016) 1126–1140, https://doi.org/10.1016/J.RSER.2015.12.185.

[11] T.M.H. Dabros, M.Z. Stummann, M. Høj, P.A. Jensen, J.-D. Grunwaldt, J. Gabrielsen, P.M. Mortensen, A.D. Jensen, Transportation fuels from biomass fast pyrolysis, catalytic hydrodeoxygenation, and catalytic fast hydropyrolysis, Prog. Energy Combust. Sci. 68 (2018) 268–309, https://doi.org/10.1016/j.pecs.2018.05.002.

[12] D.C. Elliott, Biofuel from fast pyrolysis and catalytic hydrodeoxygenation, Curr. Opin. Chem. Eng. 9 (2015) 59–65, https://doi.org/10.1016/j.coche.2015.08.008.

[13] P.M. Mortensen, J.D. Grunwaldt, P.A. Jensen, K.G. Knudsen, A.D. Jensen, A review of catalytic upgrading of bio-oil to engine fuels, Appl. Catal. A Gen. 407 (2011) 1–19, https://doi.org/10.1016/j.apcata.2011.08.046.

[14] P.M. Mortensen, J.D. Grunwaldt, P.A. Jensen, K.G. Knudsen, A.D. Jensen, A review of catalytic upgrading of bio-oil to engine fuels, Appl. Catal. A Gen. 407 (2011) 1–19, https://doi.org/10.1016/j.apcata.2011.08.046.

[15] C. Pfitzer, N. Dahmen, N. Tröger, F. Weirich, J. Sauer, A. Günther, M. Müller-Hagedorn, Fast Pyrolysis of Wheat Straw in the Bioliq pilot Plant, Energy and Fuels 30 (2016) 8047–8054, https://doi.org/10.1021/acs.energyfuels.6b01412.

[16] H.K. Mullen C, A. Boateng, N. Goldberg, I. Lima, D. Laird, Bio-oil and bio-char production from corn cobs and Stover by fast pyrolysis, Biomass Bioenergy 34 (2010) 67–74, https://doi.org/10.1016/j.biombioe.2009.09.012.

[17] S. Vecino Mantilla, P. Gauthier-Maradei, P. Álvarez Gil, S. Tarazona Cárdenas, Comparative study of bio-oil production from sugarcane bagasse and palm empty fruit bunch: Yield optimization and bio-oil characterization, J. Anal. Appl. Pyrolysis 108 (2014) 284–294, https://doi.org/10.1016/j.jaap.2014.04.003.

[18] Z. Anwar, M. Gulfraz, M. Irshad, Agro-industrial lignocellulosic biomass a key to unlock the future bio-energy: A brief review, J. Radiat. Res. Appl. Sci. 7 (2014) 163–173, https://doi.org/10.1016/j.jrras.2014.02.003.

[19] M.R. Islam, M. Parveen, H. Haniu, Properties of sugarcane waste-derived bio-oils obtained by fixed-bed fire-tube heating pyrolysis, Bioresour. Technol. 101 (2010) 4162–4168, https://doi.org/10.1016/j.biortech.2009.12.137.

[20] A. Dewangan, D. Pradhan, R.K. Singh, Co-pyrolysis of sugarcane bagasse and low-density polyethylene: Influence of plastic on pyrolysis product yield, Fuel 185 (2016) 508–516, https://doi.org/10.1016/j.fuel.2016.08.011.

[21] R.H. Venderbosch, A.R. Ardiyanti, J. Wildschut, A. Oasmaa, H.J. Heeres, Stabilization of biomass-derived pyrolysis oils, J. Chem. Technol. Biotechnol. 85 (2010) 674–686, https://doi.org/10.1002/jctb.2354.

[22] T. Kan, V. Strezov, T.J. Evans, Lignocellulosic biomass pyrolysis: A review of product properties and effects of pyrolysis parameters, Renew. Sust. Energ. Rev. 57 (2016) 126–1140, https://doi.org/10.1016/j.rser.2015.12.185.

[23] M. Saidi, F. Samimi, D. Karimipourfard, T. Nimmanwudipong, B.C. Gates, M.R. Rahimpour, Upgrading of lignin-derived bio-oils by catalytic hydrodeoxygenation, Energy Environ. Sci. 7 (2014) 103–129, https://doi.org/10.1039/C3EE43081B.

[24] Z. Sun, B. Fridrich, A. De Santi, S. Elangovan, K. Barta, Bright Side of Lignin Depolymerization: toward New Platform Chemicals, Chem. Rev. 118 (2018) 614–678, https://doi.org/10.1021/acs.chemrev.7b00588.

[25] H. Shi, J. Chen, Y. Yang, S. Tian, Catalytic deoxygenation of methyl laurate as a model compound to hydrocarbons on nickel phosphide catalysts: Remarkable support effect, Fuel Process. Technol. 118 (2014) 161–170, https://doi.org/10.1016/j.fuproc.2013.08.010.

[26] A. Sápi, R. Rémiás, Z. Kónya, Á. Kukovecz, K. Kordás, I. Kiricsi, Synthesis and characterization of nickel catalysts supported on different carbon materials, React. Kinet. Catal. Lett. 96 (2009) 379–389, https://doi.org/10.1007/s11144-009-5527-3.

[27] H. Jahromi, F.A. Agblevor, Hydrotreating of guaiacol: A comparative study of Red mud-supported nickel and commercial Ni/SiO2-Al2O3 catalysts, Appl. Catal. A Gen. 558 (2018) 109–121, https://doi.org/10.1016/j.apcata.2018.03.016.

[28] S. Jin, Z. Xiao, C. Li, X. Chen, L. Wang, J. Xing, W. Li, C. Liang, Catalytic hydrodeoxygenation of anisole as lignin model compound over supported nickel catalysts, Catal. Today 234 (2014) 125–132, https://doi.org/10.1016/j.cattod.2014.02.014.

[29] C.C. Schmitt, M.G. Reolon, M. Zimmermann, K. Raffelt, J.-D. Grunwaldt, N. Dahmen, Synthesis and Regeneration of Nickel-based Catalysts for Hydrodeoxygenation of Beech Wood Fast Pyrolysis Bio-Oil, Catalysts 8 (2018) 449, https://doi.org/10.3390/catal8100449.

[30] H. Jahromi, F.A. Agblevor, Hydrodeoxygenation of pinyon-juniper catalytic pyrolysis oil using red mud-supported nickel catalysts, Appl. Catal. B Environ. 236 (2018) 1–12, https://doi.org/10.1016/j.apcatb.2018.05.008.

[31] S. Phimsen, W. Kiatkittipong, H. Yamada, T. Tagawa, K. Kiatkittipong, N. Laosiripojana, S. Assabumrungrat, Nickel sulfide, nickel phosphide and nickel carbide catalysts for bio-hydrotreated fuel production, Energy Convers. Manag. 151 (2017) 324–333, https://doi.org/10.1016/j.enconman.2017.08.089.

[32] V.A. Yakovlev, M.V. Bykova, S.A. Khromova, Stability of nickel-containing catalysts for hydrodeoxygenation of biomass pyrolysis products, Catal. Ind. 4 (2012) 324–339, https://doi.org/10.1134/S2070050412040204.

[33] W.C.T. Vitidsantbc, Upgrading bio-oil produced from the catalytic pyrolysis of sugarcane (Saccharum officinarum L) straw using calcined dolomite, Sustain.

Chem. Pharm. 6 (2017) 114–123, https://doi.org/10.1016/j.scp.2017.10.005.
[34] J.C. del Río, A.G. Lino, J.L. Colodette, C.F. Lima, A. Gutiérrez, Á.T. Martínez, F. Lu, J. Ralph, J. Rencoret, Differences in the chemical structure of the lignins from sugarcane bagasse and straw, Biomass Bioenergy 81 (2015) 322–338, https://doi.org/10.1016/j.biombioe.2015.07.006.
[35] S. Al Arni, Extraction and isolation methods for lignin separation from sugarcane bagasse: A review, Ind. Crop. Prod. 115 (2018) 330–339, https://doi.org/10.1016/j.indcrop.2018.02.012.
[36] D. Mohan, C.U. Pittman, P.H. Steele, Pyrolysis of Wood/Biomass for Bio-oil: A critical Review, Energy Fuel 20 (2006) 848–889, https://doi.org/10.1021/ef0502397.
[37] Agência Brasil, Etanol deve alcançar recorde de produção com 33,14 bilhões de litros, Agência Bras, http://agenciabrasil.ebc.com.br/economia/noticia/2019-04/etanol-deve-alcancar-recorde-de-producao-com-3358-bilhoes-de-litros, (2019) , Accessed date: 22 May 2019.
[38] J. Moss, What to expect from Brazil's RenovaBio programme, Energy Blog (2018), https://knect365.com/energy/article/e5560843-78a9-4034-81f7-25319afe103c/what-to-expect-from-brazils-renovabio-programme , Accessed date: 22 May 2019.
[39] A. Maria, M. Alves, Mediante Pirólisis Analítica En Madera De Pinus Caribaea. Content and Quality Study of the Lignin by Analytical Pyrolysis in Pinus Caribaea, Quality 9 (2007) 179–188, https://doi.org/10.4067/S0718-221X2007000200008.
[40] A. Alves, M. Schwanninger, H. Pereira, J. Rodrigues, Analytical pyrolysis as a direct method to determine the lignin content in wood: part 1: Comparison of pyrolysis lignin with Klason lignin, J. Anal. Appl. Pyrolysis 76 (2006) 209–213, https://doi.org/10.1016/j.jaap.2005.11.004.
[41] A. Funke, D. Richter, A. Niebel, N. Dahmen, J. Sauer, Fast Pyrolysis of Biomass Residues in a Twin-screw Mixing Reactor, J. Vis. Exp. (2016), https://doi.org/10.3791/54395.
[42] A. Funke, M. Tomasi, N. Dahmen, H. Leibold, Experimental comparison of two bench scale units for fast and intermediate pyrolysis, J. Anal. Appl. Pyrolysis 124 (2017) 504–514, https://doi.org/10.1016/j.jaap.2016.12.033.
[43] A. Funke, R. Grandl, M. Ernst, N. Dahmen, Modelling and improvement of heat transfer coefficient in auger type reactors for fast pyrolysis application, Chem. Eng. Process. - Process Intensif. 130 (2018) 67–75, https://doi.org/10.1016/j.cep.2018.05.023.
[44] C.C. Schmitt, K. Raffelt, A. Zimina, B. Krause, T. Otto, M. Rapp, J.D. Grunwaldt, N. Dahmen, Hydrotreatment of Fast Pyrolysis Bio-oil Fractions over Nickel-based Catalyst, Top. Catal. 0 (2018) 0. doi:https://doi.org/10.1007/s11244-018-1009-z.
[45] W. Yin, A. Kloekhorst, R.H. Venderbosch, M.V. Bykova, S.A. Khromova, V.A. Yakovlev, H.J. Heeres, Catalytic hydrotreatment of fast pyrolysis liquids in batch and continuous set-ups using a bimetallic Ni–Cu catalyst with a high metal content, Catal. Sci. Technol. 6 (2016) 5899–5915, https://doi.org/10.1039/C6CY00503A.
[46] S.A. Channiwala, P.P. Parikh, A unified correlation for estimating HHV of solid, liquid and gaseous fuels, Fuel 81 (2002) 1051–1063, https://doi.org/10.1016/S0016-2361(01)00131-4.
[47] M. Windt, D. Meier, J.H. Marsman, H.J. Heeres, S. de Koning, Micro-pyrolysis of technical lignins in a new modular rig and product analysis by GC-MS/FID and GC × GC-TOFMS/FID, J. Anal. Appl. Pyrolysis 85 (2009) 38–46, https://doi.org/10.1016/j.jaap.2008.11.011.
[48] C. Boscagli, K. Raffelt, J.D. Grunwaldt, Reactivity of platform molecules in pyrolysis oil and in water during hydrotreatment over nickel and ruthenium catalysts, Biomass Bioenergy 106 (2017) 63–73, https://doi.org/10.1016/j.biombioe.2017.08.013.
[49] A.K. Varma, P. Mondal, Pyrolysis of sugarcane bagasse in semi batch reactor: Effects of process parameters on product yields and characterization of products, Ind. Crop. Prod. 95 (2017) 704–717, https://doi.org/10.1016/j.indcrop.2016.11.039.
[50] J. Augustínová, Z. Cvengrošová, J. Mikulec, B. Vasilkovová, J. Cvengroš, F. Stu, Upgrading of biooil from fast pyrolysis, 46th Int. Conf. Pet. Process, vol. 7, 2013.
[51] A. Oasmaa, Y. Solantausta, V. Arpiainen, E. Kuoppala, K. Sipilä, Fast pyrolysis bio-oils from wood and agricultural residues, Energy and Fuels 24 (2010) 1380–1388, https://doi.org/10.1021/ef901107f.
[52] Nicole Tröger, Daniel Richter, Ralph Stahl, Effect of feedstock composition on product yields and energy recovery rates of fast pyrolysis products from different straw types, J. Anal. Appl. Pyrolysis 100 (2013) 158–165, https://doi.org/10.1016/j.jaap.2012.12.012.
[53] S.D. Rabiu, M. Auta, A.S. Kovo, An upgraded bio-oil produced from sugarcane bagasse via the use of HZSM-5 zeolite catalyst, Egypt. J. Pet. (2018) 1–6, https://doi.org/10.1016/j.ejpe.2017.09.001.
[54] V. Sukumar, V. Manieniyan, S. Sivaprakasam, Bio oil production from biomass using pyrolysis and upgrading - A review, Int. J. ChemTech Res. 8 (2015) 196–206.
[55] C.H. Bartholomew, Mechanisms of catalyst deactivation, Appl. Catal. A Gen. 212 (2001) 17–60, https://doi.org/10.1016/S0926-860X(00)00843-7.
[56] C. Boscagli, C. Yang, A. Welle, W. Wang, S. Behrens, K. Raffelt, J.D. Grunwaldt, Effect of pyrolysis oil components on the activity and selectivity of nickel-based catalysts during hydrotreatment, Appl. Catal. A Gen. 544 (2017) 161–172, https://doi.org/10.1016/j.apcata.2017.07.025.
[57] C. Boscagli, M. Tomasi Morgano, K. Raffelt, H. Leibold, J.-D. Grunwaldt, Influence of feedstock, catalyst, pyrolysis and hydrotreatment temperature on the composition of upgraded oils from intermediate pyrolysis, Biomass Bioenergy 116 (2018) 236–248, https://doi.org/10.1016/j.biombioe.2018.06.022.
[58] F.J.F. Lopes, F.O. Silvério, D.C.F. Baffa, M.E. Loureiro, M.H.P. Barbosa, Determination of Sugarcane Bagasse Lignin S/G/H Ratio by Pyrolysis GC/MS, J. Wood Chem. Technol. 31 (2011) 309–323, https://doi.org/10.1080/02773813.2010.550379.
[59] J.L. Banyasz, S. Li, J.L. Lyons-Hart, K.H. Shafer, Cellulose pyrolysis: the kinetics of hydroxyacetaldehyde evolution, J. Anal. Appl. Pyrolysis 57 (2001) 223–248, https://doi.org/10.1016/S0165-2370(00)00135-2.
[60] S. Oh, G. Choi, J. Kim, Production of acetic acid-rich bio-oils from the fast pyrolysis of biomass and synthesis of calcium magnesium acetate deicer, J. Anal. Appl. Pyrolysis 124 (2017) 122–129, https://doi.org/10.1016/j.jaap.2017.01.032.
[61] D. Shen, W. Jin, J. Hu, R. Xiao, K. Luo, An overview on fast pyrolysis of the main constituents in lignocellulosic biomass to valued-added chemicals: Structures, pathways and interactions, Renew. Sust. Energ. Rev. 51 (2015) 761–774, https://doi.org/10.1016/j.rser.2015.06.054.
[62] A.M. Azeez, D. Meier, J. Odermatt, Temperature dependence of fast pyrolysis volatile products from European and African biomasses, J. Anal. Appl. Pyrolysis 90 (2011) 81–92, https://doi.org/10.1016/j.jaap.2010.11.005.
[63] J.D. Martínez, A. Veses, A.M. Mastral, R. Murillo, M.V. Navarro, N. Puy, A. Artigues, J. Bartrolí, T. García, Co-pyrolysis of biomass with waste tyres: Upgrading of liquid bio-fuel, Fuel Process. Technol. 119 (2014) 263–271, https://doi.org/10.1016/j.fuproc.2013.11.015.
[64] P.R. Patwardhan, Understanding the product distribution from biomass fast pyrolysis, Chem. Eng. Ph. D. (2010) 162 (doi:Doctoral Thesis).
[65] J.S. Lupoi, S. Singh, R. Parthasarathi, B.A. Simmons, R.J. Henry, Recent innovations in analytical methods for the qualitative and quantitative assessment of lignin, Renew. Sust. Energ. Rev. 49 (2015) 871–906, https://doi.org/10.1016/j.rser.2015.04.091.
[66] X. Lin, S. Sui, S. Tan, C. Pittman, J. Sun, Z. Zhang, Fast Pyrolysis of four Lignins from Different Isolation Processes using Py-GC/MS, Energies 8 (2015) 5107–5121, https://doi.org/10.3390/en8065107.
[67] S. Wu, Estimation and Comparison of Bio-Oil Components from Different Pyrolysis Conditions, vol. 3, (2015), pp. 1–11, https://doi.org/10.3389/fenrg.2015.00028.
[68] A. Poelking, Viviane Guzzo De Carli, M.E. Ricci-Silva Giordano, T.C.R. Williams, D.A. Peçanha, M.C. Ventrella, J. Rencoret, J. Ralph, M.H.P. Barbosa, M. Loureiro, Analysis of a modern hybrid and an ancient sugarcane implicates a complex interplay of factors in affecting recalcitrance to cellulosic ethanol production, PLoS One 10 (2015), https://doi.org/10.1371/journal.pone.0134964.
[69] A. Oasmaa, E. Kuoppala, S. Gust, Y. Solantausta, Extractives on phase Separation of Pyrolysis Liquids, Energy Fuel 17 (2003).
[70] A.A.U. George W. Huber David M. Ford, Surita R. Bhatia, Phillip C. Badger, Fast Pyrolysis Oil Stabilization: An Integrated Catalytic and Membrane Approach for Improved Bio-Oils, (2011) 72. http://www.osti.gov/scitech//servlets/purl/1053421/.
[71] S. Oh, H.S. Choi, I.-G. Choi, J.W. Choi, Evaluation of hydrodeoxygenation reactivity of pyrolysis bio-oil with various Ni-based catalysts for improvement of fuel properties, RSC Adv. 7 (2017) 15116–15126, https://doi.org/10.1039/C7RA01166K.
[72] C. Boscagli, K. Raffelt, T.A. Zevaco, W. Olbrich, T.N. Otto, J. Sauer, J.D. Grunwaldt, Mild hydrotreatment of the light fraction of fast-pyrolysis oil produced from straw over nickel-based catalysts, Biomass Bioenergy 83 (2015) 525–538, https://doi.org/10.1016/j.biombioe.2015.11.003.
[73] D.C. Elliott, T.R. Hart, Catalytic hydroprocessing of chemical models for bio-oil, Energy and Fuels 23 (2009) 631–637, https://doi.org/10.1021/ef8007773.
[74] J.A. Mercader, F. D. M.; Koehorst, P. J. J.; Heeres, H.J.; Kersten, S. R. A.; Hogendoorn, Competition between Hydrotreating and Polymerization Reactions during Pyrolysis Oil Hydrodeoxygenation, AICHE J. 55 (2011) 3160–3170. doi:https://doi.org/10.1002/aic.12503.
[75] W. Yin, A. Kloekhorst, R.H. Venderbosch, M.V. Bykova, S.A. Khromova, V.A. Yakovlev, H.J. Heeres, Catalytic hydrotreatment of fast pyrolysis liquids in batch and continuous set-ups using a bimetallic Ni-Cu catalyst with a high metal content, Catal. Sci. Technol. 6 (2016) 5899–5915, https://doi.org/10.1039/c6cy00503a.
[76] A. Kloekhorst, H.J. Heeres, Catalytic Hydrotreatment of Alcell Lignin using Supported Ru, Pd, and Cu Catalysts, ACS Sustain. Chem. Eng. 3 (2015) 1905–1914, https://doi.org/10.1021/acssuschemeng.5b00041.
[77] X.X. Jiang, E. Naoko, Z.P. Zhong, Structure properties of pyrolytic lignin extracted from aged bio-oil, Chin. Sci. Bull. 56 (2011) 1417–1421, https://doi.org/10.1007/s11434-011-4465-4.
[78] A.R.K. Gollakota, M. Reddy, M.D. Subramanyam, N. Kishore, A review on the upgradation techniques of pyrolysis oil, Renew. Sust. Energ. Rev. 58 (2016) 1543–1568, https://doi.org/10.1016/j.rser.2015.12.180.
[79] W. Yin, R. Hendrikus, M.V. Alekseeva, M. Bernardes, H. Heeres, A. Khromova, V.A. Yakovlev, C. Cannilla, G. Bonura, F. Frusteri, H. Jan, Hydrotreatment of the Carbohydrate-Rich Fraction of Pyrolysis Liquids Using Bimetallic Ni Based Catalyst: Catalyst Activity and Product Property Relations, vol. 169, (2018), pp. 258–268, https://doi.org/10.1016/j.fuproc.2017.10.006.
[80] R.J. French, J. Stunkel, S. Black, M. Myers, M.M. Yung, K. Iisa, Evaluate impact of catalyst type on oil yield and hydrogen consumption from mild hydrotreating, Energy and Fuels 28 (2014) 3086–3095, https://doi.org/10.1021/ef4019349.
[81] F.D.M. Mercader, Pyrolysis Oil Upgrading for Co-Processing in Standard Refinery Units, University of Twente F, 2010, https://doi.org/10.3990/1.9789036530859.
[82] J. Payormhorm, K. Kangvansaichol, P. Reubroycharoen, P. Kuchonthara, N. Hinchiranan, Pt/Al2O3-catalytic deoxygenation for upgrading of Leucaena leucocephala-pyrolysis oil, Bioresour. Technol. 139 (2013) 128–135, https://doi.org/10.1016/j.biortech.2013.04.023.
[83] D.C. Elliott, Historical developments in hydroprocessing bio-oils, Energy and Fuels 21 (2007) 1792–1815, https://doi.org/10.1021/ef070044u.

[84] C.A. Mullen, G.D. Strahan, A.A. Boateng, Characterization of various fast-pyrolysis bio-oils by NMR spectroscopy, Energy and Fuels 23 (2009) 2707–2718, https://doi.org/10.1021/ef801048b.
[85] F. Stankovikj, A.G. McDonald, G.L. Helms, M. Garcia-Perez, Quantification of Bio-Oil Functional groups and Evidences of the Presence of Pyrolytic Humins, Energy and Fuels 30 (2016) 6505–6524, https://doi.org/10.1021/acs.energyfuels.6b01242.
[86] J. Wang, J. Chang, J. Fan, Catalytic esterification of bio-oil by ion exchange resins, J. Fuel Chem. Technol. 38 (2010) 560–564, https://doi.org/10.1016/S1872-5813(10)60045-X.
[87] D.E. Resasco, S. Sitthisa, J. Faria, T. Prasomsri, M.P. Ruiz, Furfurals as Chemical Platform for Biofuels Production, (2011).
[88] Z. Si, X. Zhang, C. Wang, L. Ma, R. Dong, An Overview on Catalytic Hydrodeoxygenation of Pyrolysis Oil and its Model Compounds, Catalysts 7 (2017) 169, https://doi.org/10.3390/catal7060169.
[89] H. Wan, R.V. Chaudhari, B. Subramaniam, Aqueous phase hydrogenation of acetic acid and its promotional effect on p-cresol hydrodeoxygenation, Energy and Fuels 27 (2013) 487–493, https://doi.org/10.1021/ef301400c.
[90] Y.K. Lugo-josé, J.R. Monnier, A. Heyden, C.T. Williams, Hydrodeoxygenation of propanoic acid over silica-supported palladium: effect of metal particle size, Catal. Sci. Technol. 4 (2014) 3909–3916, https://doi.org/10.1039/c4cy00605d.
[91] Z. He, X. Wang, Hydrodeoxygenation of model compounds and catalytic systems for pyrolysis bio-oils upgrading, Catal. Sustain. Energy. 1 (2012) 28–52, https://doi.org/10.2478/cse-2012-0004.
[92] A.R. Ardiyanti, S.A. Khromova, R.H. Venderbosch, V.A. Yakovlev, I.V. Melián-Cabrera, H.J. Heeres, Catalytic hydrotreatment of fast pyrolysis oil using bimetallic Ni-Cu catalysts on various supports, Appl. Catal. A Gen. 449 (2012) 121–130, https://doi.org/10.1016/j.apcata.2012.09.016.
[93] R. Gunawan, X. Li, C. Lievens, M. Gholizadeh, W. Chaiwat, X. Hu, D. Mourant, J. Bromly, C.Z. Li, Upgrading of bio-oil into advanced biofuels and chemicals. Part I. Transformation of GC-detectable light species during the hydrotreatment of bio-oil using Pd/C catalyst, Fuel 111 (2013) 709–717, https://doi.org/10.1016/j.fuel.2013.04.002.
[94] R. Venderbosch, H. Heeres, Pyrolysis Oil Stabilisation by Catalytic Hydrotreatment, in: M.A. dos S. Bernardes (Ed.), Biofuel's Eng. Process Technol, InTech, 2011, pp. 385–410, , https://doi.org/10.5772/18446.
[95] A. Ardiyanti, Hydrotreatment of Fast Pyrolysis Oil: Catalyst Development and Process-Product Relations, (2013).
[96] K. Routray, K.J. Barnett, G.W. Huber, Hydrodeoxygenation of Pyrolysis oils, Energy Technol 5 (2016) 80–93, https://doi.org/10.1002/ente.201600084.
[97] K.L. Deutsch, Copper Catalysts in the C-O Hydrogenolysis of Biorenewable Compounds, Iowa State University, 2012.
[98] Y. Xu, L. Zhang, J. Chang, X. Zhang, L. Ma, T. Wang, Q. Zhang, One step hydrogenation-esterification of model compounds and bio-oil to alcohols and esters over Raney Ni catalysts, Energy Convers. Manag. 108 (2016) 78–84, https://doi.org/10.1016/j.enconman.2015.10.062.
[99] A. Witsuthammakul, T. Sooknoi, Selective hydrodeoxygenation of bio-oil derived products: ketones to olefins, Catal. Sci. Technol. 5 (2015) 3639–3648, https://doi.org/10.1039/C5CY00367A.
[100] A. Sanna, T.P. Vispute, G.W. Huber, Hydrodeoxygenation of the aqueous fraction of bio-oil with Ru/C and Pt/C catalysts, Appl. Catal. B Environ. 165 (2015) 446–456, https://doi.org/10.1016/j.apcatb.2014.10.013.
[101] R. Mariscal, P. Maireles-Torres, M. Ojeda, I. Sádaba, M. López Granados, Furfural: a renewable and versatile platform molecule for the synthesis of chemicals and fuels, Energy Environ. Sci. 9 (2016) 1144–1189, https://doi.org/10.1039/C5EE02666K.
[102] I. Gandarias, P.L. Arias, Hydrotreating Catalytic Processes for Oxygen Removal in the Upgrading of Bio-oils and Bio-Chemicals, Liq. Gaseous, Solid Biofuels-Conversion Tech. (2013) 327–356, https://doi.org/10.5772/50479.
[103] J. Kayalvizhi, A. Pandurangan, Hydrodeoxygenation of vanillin using palladium on mesoporous KIT-6 in vapour phase reactor, Mol. Catal. 436 (2017) 67–77, https://doi.org/10.1016/j.mcat.2017.04.002.
[104] F.D.M. Mercader, Pyrolysis Oil Upgrading for Co-Processing in Standard Refinery Units, (2010), https://doi.org/10.3990/1.9789036530859.
[105] R. Venderbosch, H. Heeres, Stabilisation of Biomass derived Pyrolysis oils by Catalytic Hydrotreatment, Biocoup.Com. (n.d.) 1–28. http://www.biocoup.com/fileadmin/user/december/Update_December_2011/101_RUG_BTG_March11.pdf.
[106] W. Chen, Z. Luo, Y. Yang, G. Li, J. Zhang, Q. Dang, Upgrading of Bio-oil in Supercritical Ethanol: using Furfural and Acetic Acid as Model Compounds, Bio Resources 8 (2013) 3934–3952.
[107] M.B. Figueirêdo, Z. Jotic, P.J. Deuss, R.H. Venderbosch, H.J. Heeres, Hydrotreatment of pyrolytic lignins to aromatics and phenolics using heterogeneous catalysts, Fuel Process. Technol. 189 (2019) 28–38, https://doi.org/10.1016/J.FUPROC.2019.02.020.
[108] Z. Si, X. Zhang, C. Wang, L. Ma, R. Dong, An Overview on Catalytic Hydrodeoxygenation of Pyrolysis Oil and its Model Compounds, Catalysts 7 (2017) 1–22, https://doi.org/10.3390/catal7060169.
[109] M.V. Bykova, D.Y. Ermakov, V.V. Kaichev, O.A. Bulavchenko, A.A. Saraev, M.Y. Lebedev, V. Yakovlev, Ni-based sol-gel catalysts as promising systems for crude bio-oil upgrading: Guaiacol hydrodeoxygenation study, Appl. Catal. B Environ. 113–114 (2012) 296–307, https://doi.org/10.1016/j.apcatb.2011.11.051.